Materials Today Bio 20 (2023) 100646

Contents lists available at ScienceDirect

Materials Today Bio

journal homepage: www.journals.elsevier.com/materials-today-bio

Recent advances of lanthanide nanomaterials in Tumor NIR fluorescence detection and treatment

Qi Fan [a,b,**], Chao Sun [a,b], Bingliang Hu [a], Quan Wang [a,b,*]

[a] Key Laboratory of Spectral Imaging Technology, Xi'an Institute of Optics and Precision Mechanics (XIOPM), Chinese Academy of Sciences, Xi'an, 710119, China
[b] Key Laboratory of Biomedical Spectroscopy of Xi'an, Key Laboratory of Spectral Imaging Technology, Xi'an Institute of Optics and Precision Mechanics (XIOPM), Chinese Academy of Sciences, Xi'an, 710119, China

ARTICLE INFO

Keywords:
Lanthanide nanomaterials
Medical diagnosis
Therapy
Rare earths
Near infrared window
Fluorescence imaging

ABSTRACT

Lanthanide nanomaterials have garnered significant attention from researchers among the main near-infrared (NIR) fluorescent nanomaterials due to their excellent chemical and fluorescence stability, narrow emission band, adjustable luminescence color, and long lifetime. In recent years, with the preparation, functional modification, and fluorescence improvement of lanthanide materials, great progress has been made in their application in the biomedical field. This review focuses on the latest progress of lanthanide nanomaterials in tumor diagnosis and treatment, as well as the interaction mechanism between fluorescence and biological tissues. We introduce a set of efficient strategies for improving the fluorescence properties of lanthanide nanomaterials and discuss some representative in-depth research work in detail, showcasing their superiority in early detection of ultra-small tumors, phototherapy, and real-time guidance for surgical resection. However, lanthanide nanomaterials have only realized a portion of their potential in tumor applications so far. Therefore, we discuss promising methods for further improving the performance of lanthanide nanomaterials and their future development directions.

1. Introduction

With the advancement of science and technology, interdisciplinary integration has become a prominent feature and an essential way of modern scientific development [1–10]. Medical diagnostic technology, as a crucial foundation for medical research and clinical treatment, integrates multiple new technologies, including computer science, biology, and materials science. It has become one of the fastest-growing fields in the medical industry over the last two decades [11–16]. The non-invasive, rapid and efficient diagnosis enabled by medical imaging technology has ushered in a new era of digital medicine, promoting the digitization and intelligence of medical diagnosis. Medical diagnosis and treatment aided by computer graphics and image processing technology have significantly enhanced their accuracy and safety, becoming a promising development direction of clinical medicine [17]. In the past two decades, medical diagnostic technology has developed very rapidly. The emergence of each new signal source, transmission mode and calculation method will bring the innovation of medical diagnostic technology, which plays a crucial role in promoting the development of biology and clinical medicine. Nowadays, several medical diagnostic technologies have already been developed and implemented in clinical practice, such as magnetic resonance imaging (MRI), computed tomography (CT), Photoacoustic imaging (PA), positron emission computed tomography (PET) and single-photon emission computed tomography (SPECT). These imaging modes, combined with ingenious design of various contrast agents, can carry out efficient diagnosis, treatment and monitoring of different diseases [18–20]. Among them, the low resolution and dangerous ionizing radiation of tomography imaging technology (CT, pet and SPECT), as well as the time-consuming imaging of CT, MRI, pet and SPECT, limit their real-time visualization application in disease treatment.

Fluorescence imaging has attracted more and more attention because of its lower cost, faster feedback, higher sensitivity, non-radiation, noninvasive and simpler operation compared with these medical diagnostic modes [21,22]. Since the advent of fluorescence microscopy, researchers have been continuously advancing its development through

* Corresponding author. Key Laboratory of Spectral Imaging Technology, Xi'an Institute of Optics and Precision Mechanics (XIOPM), Chinese Academy of Sciences, Xi'an, 710119, China.
** Corresponding author. Key Laboratory of Spectral Imaging Technology, Xi'an Institute of Optics and Precision Mechanics (XIOPM), Chinese Academy of Sciences, Xi'an, 710119, China.
E-mail addresses: fanqi@opt.ac.cn (Q. Fan), wangquan@opt.ac.cn (Q. Wang).

https://doi.org/10.1016/j.mtbio.2023.100646
Received 12 January 2023; Received in revised form 23 April 2023; Accepted 26 April 2023
Available online 2 May 2023

various variants and improved technologies. Until the emergence of super-resolution fluorescence microscopy, the ultimate resolution of fluorescence imaging reached tens of nanometers [23–25]. Fluorescence imaging can be used to monitor the dynamic interaction between drug molecules and cells. In particular, The NIR fluorescence imaging has negligible tissue scattering, absorption, tissue autofluorescence and high signal-to-noise ratio. It can monitor the real-time dynamic process in biological tissue [26]. Because the absorption peak of DNA is located at 260 nm and that of hemoglobin is also less than 600 nm, the penetration depth and signal-to-noise ratio in biological tissues are greatly improved when the excitation or emission light is located in the NIR range above 700 nm [27]. In 1999, The NIR imaging was first applied to the diagnosis of tumors in vivo, and the tissue penetration depth reached 1–2 cm [28]. The NIR region can be divided into NIR-I (700–900 nm) and NIR-II (1000–1700 nm). Dai's research group first explored NIR-II in 2009 [29], and its research revealed that in the NIR-II, biological tissues such as skin and fat can scatter and absorb fewer photons than the NIR-I, so this window is currently considered to be the optimal biological imaging window [30]. At present, many types of NIR-II nanomaterials have been designed for biological imaging, including semiconductor quantum dots (ZnS, PbS, PbSe, CdHgTe) [31], single-walled carbon nanotubes (SWCNTs) [32], organic small molecule dyes [33], conjugated polymers [34] and AIE materials [35]. However, some quantum dot materials (mainly containing toxic heavy metal elements such as cadmium, selenium, and lead) and single-walled carbon nanotubes have unavoidable biological toxicity. Organic small molecule fluorophores are subject to their quantum yield, and conjugated polymers and AIE materials lack sufficient photostability.

The ideal NIR imaging material is expected to satisfy the following conditions: 1) Both excitation and emission peaks are located in the NIR region (preferably the emission peak can be located in the NIR-II region), so that the photons can penetrate deep biological tissues and reduce the damage of excitation to organisms. 2) It has sufficient biocompatibility to meet the requirements of in vivo applications [36]. 3) For bioimaging materials, it is important to have both strong fluorescence intensity and long fluorescence lifetime, as well as high ion doping concentration and low implantation dose. 4) In order to ensure that it will not be quickly cleared from the kidney by renal clearance before imaging diagnosis and does not remain in the body for too long, the particle size of contrast material should be controlled between 5.5 and 150 nm. 5) It has efficient and accurate targeting ability. 6) High luminescence stability sufficient to meet the needs of long-term fluorescence monitoring in vivo.

Lanthanide nanomaterial is an ideal noninvasive biological imaging contrast agent, which can be used to image tumor cells, tissues and vessels in living bodies [37–39]. Since 2000, researchers have successively reported groundbreaking material science research that have lead to the applicability of lanthanide nanoparticles in biological framework [40–47]. The properties of Lanthanide materials greatly affect the sensitivity, resolution and detection depth of biological imaging [48–51]. Because the rare earth ions are protected by 5s and 5p orbits, the influence of environment on the fluorescence of rare earth ions is very weak, which makes its fluorescence emission spectrum sharp (high intensity, narrow emission peak) and stable. Its full width at half maxima (FWHM) is generally 10–20 nm, while the transition metal ions are generally 100 nm and the quantum dot materials are 25–40 nm, which will limit the resolution of fluorescence imaging. Because the fluorescence emission of rare earth ions belongs to atomic transition, it also has strong photobleaching resistance. In addition, the doping of different rare earth ions also makes the emission band of the contrast material more customizable, and its fluorescence emission spectrum covers the ultraviolet, visible and NIR regions [52,53]. Therefore, lanthanide nanomaterials can be used as a powerful non-invasive biological imaging contrast agent to perform high-resolution and highly sensitive fluorescence imaging in living bodies [54–58].

Recently, lanthanide materials have not only been utilized for NIR tumor diagnosis [59–61], but also combined with CT, MRI, and other

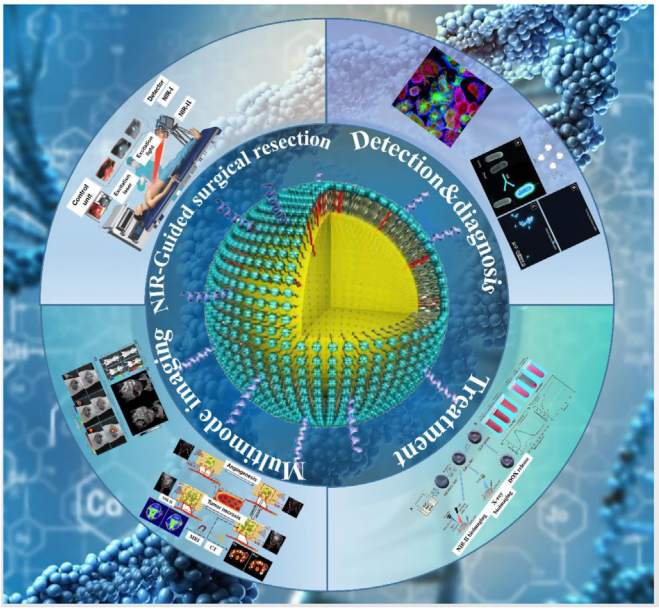

Fig. 1. Application of NIR lanthanide doped nanomaterial.

imaging contrast agents to enable multi-mode tumor imaging detection and obtain more comprehensive target tumor information [62–64]. Additionally, some lanthanide nanomaterials have greatly improved fluorescence biological penetration depth and resolution, which can be used for surgical resection guidance [65]. In order to achieve safer and non-invasive treatment, some photothermal media or photosensitizers have been physically or chemically connected to lanthanide nanomaterials to enable photothermal and photodynamic therapy for tumors [66–68]. Moreover, Lanthanide nanomaterials can also be employed as drug carriers for tumor therapy by ingeniously designing them to release drugs in a controlled and efficient manner in response to various stimuli such as pH, NIR light, and specific chemicals [69,70]. Overall, lanthanide nanomaterials have shown immense potential in the diagnosis and treatment of tumors, leading many researchers to study and make significant application progress in recent years (Fig. 1) [3,4,71–74].

2. Principle of fluorescence diagnosis

In fluorescence diagnosis, excitation light interacts with the contrast agents in biological tissues, organs or tumors [75]. The resulting fluorescence signal is transmitted to a detector and processed by a computer to generate morphological and structural information of the biological tissue, organ or tumor [76]. However, visible light is significantly absorbed or scattered by water, skin tissue, and blood, resulting in rapid attenuation of the fluorescence signal. This attenuation effect is proportional to the depth of the target detection position, and the tissue penetration depth of visible light is usually only about 1–3 mm. Thus, traditional visible light fluorescent contrast agents are inadequate for imaging detection in deeper tissues. Fortunately, NIR-II fluorescence imaging provides significant advantages over the visible region and NIR-I imaging due to the special interaction mechanism between photons and biological tissues. During the imaging process of biological tissues, the excitation and emission photons mainly exhibit the following four phenomena.

2.1. Absorption

Light absorption of biological tissue is a basic form of interaction between light and biological tissue. It refers to the process of light intensity attenuation caused by the conversion of some of its energy into

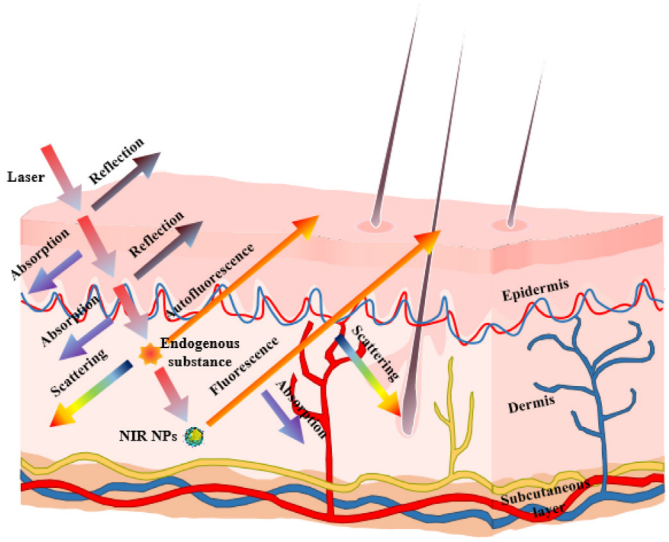

Fig. 2. Schematic diagram of light transmission in biological tissues.

stimulated radiation, as well as the conversion of the remaining energy into heat or molecular vibrations as it passes through tissue. The light intensity decreases with the increase of the transmission distance of light in the tissue, and the unabsorbed light passes out along the boundary of the tissue (Fig. 2). The substances with absorption peaks from ultraviolet to infrared in organisms mainly include water, hemoglobin, blood glucose, pigment in skin, myoglobin in muscle and cytochrome. Compared to the visible region, the absorption in the NIR region is much lower, making it the preferred window for fluorescence imaging.

2.2. Light scattering

We know that all substances are composed of molecules and atoms, and at the atomic scale, there is no absolute uniformity. When there is a significant difference in refractive index within a small part of tissue, whose size is comparable to the wavelength of visible light, the light not only reflects and refracts according to geometric optical laws but also scatters. This strong scattering of light in biological tissue is due to the micro-heterogeneity of refractive index. Research has shown that the scattering of biological tissues generally follows an inverse relationship with wavelength, but the scattering index varies with different tissues. Thus, in fluorescence diagnosis, the longer the wavelength, the lower the background noise generated by scattering. When both excitation light and emission light are located in the NIR band, the better signal-to-noise ratio and image quality can be obtained.

2.3. Reflection

The excitation light is partially reflected at the interface due to the refractive index difference between the medium and the tissue. The reflection process depends on the incident angle and refractive index difference. According to Fresnel equation, since the refractive index changes very little with wavelength, there is not much difference in reflection between NIR excitation and visible excitation, and the adjustable excitation power can also modify the process to a certain extent. Due to the rough interface, the random reflection of emitted light will produce a lot of background noise, which will interfere with the final imaging signal-to-noise ratio.

2.4. Autofluorescence

The fluorescence emitted by the inherent fluorophores in biological tissues that absorb a certain wavelength of light is called autofluorescence. Because the ground state has different vibrational energy levels, different tissues composed of different substances will emit characteristic fluorescence at different wavelengths. The autofluorescence emitted by the same tissue irradiated by different wavelengths of laser is also different. Due to the different types and quantities of fluorescent substances contained in different tissues, even when excited by the same wavelength laser, they will produce different autofluorescence [77,78]. Recent studies have shown that the use of longer wavelength light can relatively reduce the autofluorescence of some organs and body fluids [79]. In the NIR band, especially in the NIR-IIb, the autofluorescence produced by the liver, spleen and other organs can even be completely eliminated. Therefore, using this band for imaging can significantly reduce the interference of background signal, so as to greatly improve the tissue penetration depth of imaging and realize the high-quality imaging detection of deeper biological tissue.

3. Enhancement of fluorescence intensity

The improvement of the fluorescence intensity of lanthanide nanomaterials can significantly impact their range and effectiveness in biological applications [80–82]. Currently, the main methods reported to significantly improve the fluorescence efficiency of lanthanide nanomaterials include core-shell structure, dye sensitization and surface plasmon resonance (SPR) effect (Table 1).

3.1. Core-shell structure

Coating a shell on lanthanide nanomaterials can effectively inhibit the surface quenching, passivate the lattice defects on the core surface and isolate the interference of external adverse factors. As a result, the coating of a shell on lanthanide nanomaterials can be an important tool for enhancing their fluorescence properties [99].

Lanthanide core-shell structure materials consist of nano-sized particles as the core, which are then coated with one or more layers of uniform materials to form the shell (Fig. 3I) [39]. The core and the shell are connected by physical electrostatic attraction or chemical bond. Depending on the activity of the shell (whether lanthanide ions are doped in the shell), the core-shell structure can be divided into inert (undoped lanthanide ions) core-shell structure [100,101] and active (doped lanthanide ions) core-shell structure [88,89,102–104]. The inert shell can also be classified into homogeneous core-shell [105,106] structure and heterogeneous core-shell structure [83,107] according to whether the main lattice of core and shell materials is the same. Core-shell lanthanide nanomaterials can effectively reduce the quenching effect of hanging bonds and polymer vibrating groups on the fluorescence of nanomaterials, so as to effectively improve the fluorescence efficiency.

Compared with the uncoated nanoparticles $NaYF_4$:Nd, the fluorescence intensities of core-shell nanoparticles $NaYF_4$:Nd@$NaDyF_4$ prepared by Wang's research group at 1058 nm and 1332 nm were increased by 3.46 and 1.75 times respectively (Fig. 3II) [83]. Using the same inert shell strategy, Chen's team reported a new type of Er^{3+} sensitized core-shell nanocrystal $NaErF_4$:Yb^{3+}@$NaLuF_4$ (Fig. 3III), which emits efficient fluorescence at 1525 nm under 808 nm excitation without any local heating. The inert shell can inhibit the concentration dependent quenching and allow 100% Er^{3+} to be doped into the nanocrystal, resulting in about 650 times higher SWIR fluorescence than that without shell. Finally, the high-efficiency short wave NIR fluorescence with the quantum yield of 11% was realized [84]. With the further study of the core-shell structure, it is found that the thickness of the shell affects the fluorescence efficiency of the nanomaterial to some extent [108]. Li's research group designed a series of NIR nanoparticles with different doping ratios ($NaErF_4$:Ce@$NaYbF_4$@$NaLuF_4$) (Fig. 3IV). The existence of the outermost inert shell $NaLuF_4$ greatly inhibits the surface fluorescence quenching of Er^{3+}. By changing the thickness of the intermediate layer and the ion doping type of the active layer, the fluorescence intensity at 1525 nm was increased by 13.4 times, and the fluorescence lifetime was

Table 1
Summary of fluorescence enhancement methods and effects of lanthanide nanomaterials.

Composition	Emission enhancement method	Size/nm	λex/nm	λem/nm	Emission increase multiple	Ref.
$NaYF_4:Nd^{3+}$	Inert heterogeneous shell coated ($NaDyF_4$)	12.6/15.7	808	1058/1332	3.46/1.75	[83]
$NaErF_4:Yb^{3+}$	Inert heterogeneous shell coated ($NaLuF_4$)	25.5/40.7	808	1525	650	[84]
$NaErF_4:Ce^{3+}$	Inert heterogeneous shell coated ($NaLuF_4$)	12.5	808	1525	13.4	[65]
$NaGdF_4$:5%Nd	Inert homogeneous shell coated (NaGdF4)	4.38/5.3	808	1060	–	[85]
$NaGdF_4$:3%Nd	Inert homogeneous shell coated (aGdF4)	11/15	740	900	1.82	[86]
$NaYbF_4$:Tm	Active shell coated ((aGdF4:Yb)	13.23	980	800	7.2	[87]
$NaErF_4$:Tm	Active shell coated (NaGdF4:Yb)	29.8/32.1	980	654	20	[88]
$NaYF_4$:Yb,Er,Nd	Active shell coated ($NaYF_4$:Nd)	24/48	808	658	20	[89]
$NaGdF_4$:Yb,Er@$NaGdF_4$:Yb, Nd	Dye sensitization (IR-792)	28-29/32-33	808	545	4	[90]
$NaYF_4$:20%Yb^{3+},2%Er^{3+}@$NaYF_4$:10%Nd^{3+}/10%Yb^{3+}	Dye sensitization (IR-792)	19/31	785	541/654	135	[91]
$NaYF_4:Yb^{3+}/Er^{3+}$@$NaYbF_4$@$NaYF_4:Nd^{3+}$	Dye sensitization (ICG)	52	800	1530	4	[92]
$NaYbF_4$@$NaYF_4$:Nd	Dye sensitization (CY7)	18.52	808	980	15	[93]
$NaYF_4$:Yb/Tm@$NaYF_4$:Nd	Dye sensitization (IR-808)	/	808	1340	28/5	[94]
$NaYF_4$:Yb/Er/Ce@$NaYF_4$:Nd	Dye sensitization (Alk-pi)	49	808	1525	40	[95]
NYF@SiO_2	SPR effect (Au)	120	980	475	7.35	[96]
Ag/$YVO_4:Yb^{3+}$, Er^{3+}	SPR effect (Ag)	15	980	500–600	30–36	[97]
$NaYF_4$:Yb,Er,Gd	SPR effect (Au)	100–150	980	665	10	[98]

increased from 0.28 ms to 2.88 ms [65]. By changing the synthesis conditions, Zhang controlled the thickness of the nanoparticle shell (Fig. 3V), so that the fluorescence lifetime of the nanoparticle can be adjusted according to the imaging needs. Finally, combined with the time gate technology, the fluorescence imaging with high signal-to-noise ratio was obtained [100].

Another reason why core-shell strategy can be used as a commonly used method to enhance the luminescence efficiency of lanthanide materials is that it can optimize the energy transfer process of lanthanide ions between layers [109]. In 2017, Dai et al. designed a β-phase core-shell structure nanoion $NaYbF_4$:2%Er,2%Ce@$NaYF_4$, in which Ce^{3+} plays a key role. It inhibited the up-conversion luminescence of Er^{3+}, thus enhancing the down-conversion luminescence of 1550 nm, and reached 9 times the intensity before doping. The maximum quantum yield reached 2.73%, which was the highest among the conversion materials of the same type at that time [110]. In another structure ($NaYbF_4$:Tm@-$NaGdF_4$:xYb), the Yb^{3+} doped shell layer can serve as a sensitizer to transfer the absorbed near-infrared light to the core layer, resulting in an emission intensity twice that of the original. Therefore, $NaYbF_4$:Tm@$NaGdF_4$:xYb exhibits stronger NIR emission [87].

3.2. Dye sensitization

The absorption cross-section of lanthanide ions is typically weak, but this can be compensated for by the large and wide absorption bandwidth of organic dyes. By combining lanthanide nanoparticles with organic dyes, efficient energy transfer can be achieved through antenna action, resulting in enhanced fluorescence [95,111–115]. Nowadays, there are many kinds of organic dyes used to sensitize lanthanide nanomaterials, most of which are small organic molecules excited and emitted in the NIR region. Generally, their absorption peak is at 780–810 nm, and their emission peak is at 750–1150 nm. This band range coincides with the absorption peaks of Yb^{3+} (980 nm) and Nd^{3+} (740/808 nm) which commonly used as sensitizers in lanthanide nanomaterials. Thereby enabling the energy conversion from organic dyes to lanthanide materials without radiation [90].

Dye sensitization is actually more favor to improve the performance of smaller size lanthanide nanomaterials. Ultrasmall lanthanide nanomaterials (10 nm) are suitable for biological applications due to their low toxicity, but their quenching probability is high and their luminous efficiency is low. Fortunately, the dye sensitization strategy is particularly useful for improving the luminescence intensity of small-sized lanthanide nanomaterials, which is an ideal choice for their biomedical applications [116]. Although dye sensitization is an effective strategy to enhance the luminescence of lanthanide nanomaterials, the sensitization effect is limited due to the possibility of dye aggregation [117]. In order to solve this problem, the tetrastyrene groups were introduced into cyanine dyes, which not only suppressed the close packing of cyanine dyes on the surface of nanomaterials, but also improved the fluorescence quantum yield (Fig. 4I). The results show that the luminescence of dye-sensitized nanomaterials is enhanced 135 times under 785 nm excitation with a power density of 5 W cm^{-2} [91].

ICG is a commonly used candidate for dye sensitization [118,119]. An epitaxial $NaYF_4:Yb^{3+}/X^{3+}$@$NaYbF_4$@$NaYF_4:Nd^{3+}$ (X = null, Er, Ho, Tm, or Pr) core/shell/shell (CSS) nanocrystals and indocyanine green (ICG) constitute an efficient dye sensitization system. This system is able to produce a set of narrow band emissions with a large Stokes-shift (>200 nm) in the second biological window of optical transparency (NIR-II, 1000–1700 nm), by transferring directional energy from light-harvesting surface ICG, via lanthanide ions in the shells, to the emitter X^{3+} in the core (Fig. 4II). ICG on the surface not only increases the NIR-II emission intensity of the materials by 4 times, but also provides a wide range of excitable spectra (700–860 nm), which promotes their application in biomedical applications [92].

In recent years, a more efficient sensitizer Cy7 was considered to replace the commonly used sensitizer ICG. Because the quantum yield of Cy7 is higher, the sensitization effect is better than that of ICG (Fig. 4III). Cy7 sensitized NIR lanthanide nanomaterials have been demonstrated to have deep tissue penetration and low power excitation bioimaging. It has been successfully applied in blood vessel imaging and fluorescence-guided peritumoral lymph node dissection in a mouse model [93].

3.3. Surface plasmon resonance effect

SPR is an effective method to enhance the fluorescence efficiency of nano materials [120,121]. This phenomenon occurs when the frequency of incident light matches the vibration frequency of free electrons on the surface of metal nanoparticles under electromagnetic radiation, leading to their collective oscillation. As a result, SPR can significantly improve the fluorescence of these nanomaterials.

There are two modes of free electron transmission: the first is the transmission on the surface of metal film, which is called diffusion SPR, the second is the transmission on the surface of metal nanoparticles, which is called local SPR [122]. Metal nanoparticles can form a strong electric field in the sub wavelength region of the metal surface, which can greatly enhance the excitation light at the plasma resonance frequency. At the same time, it can shorten the lifetime of the excited state, enhance the radiation attenuation rate, and finally improve the fluorescence efficiency of the material. The phenomenon of metal enhanced fluorescence was first discovered and theoretically explained and verified by

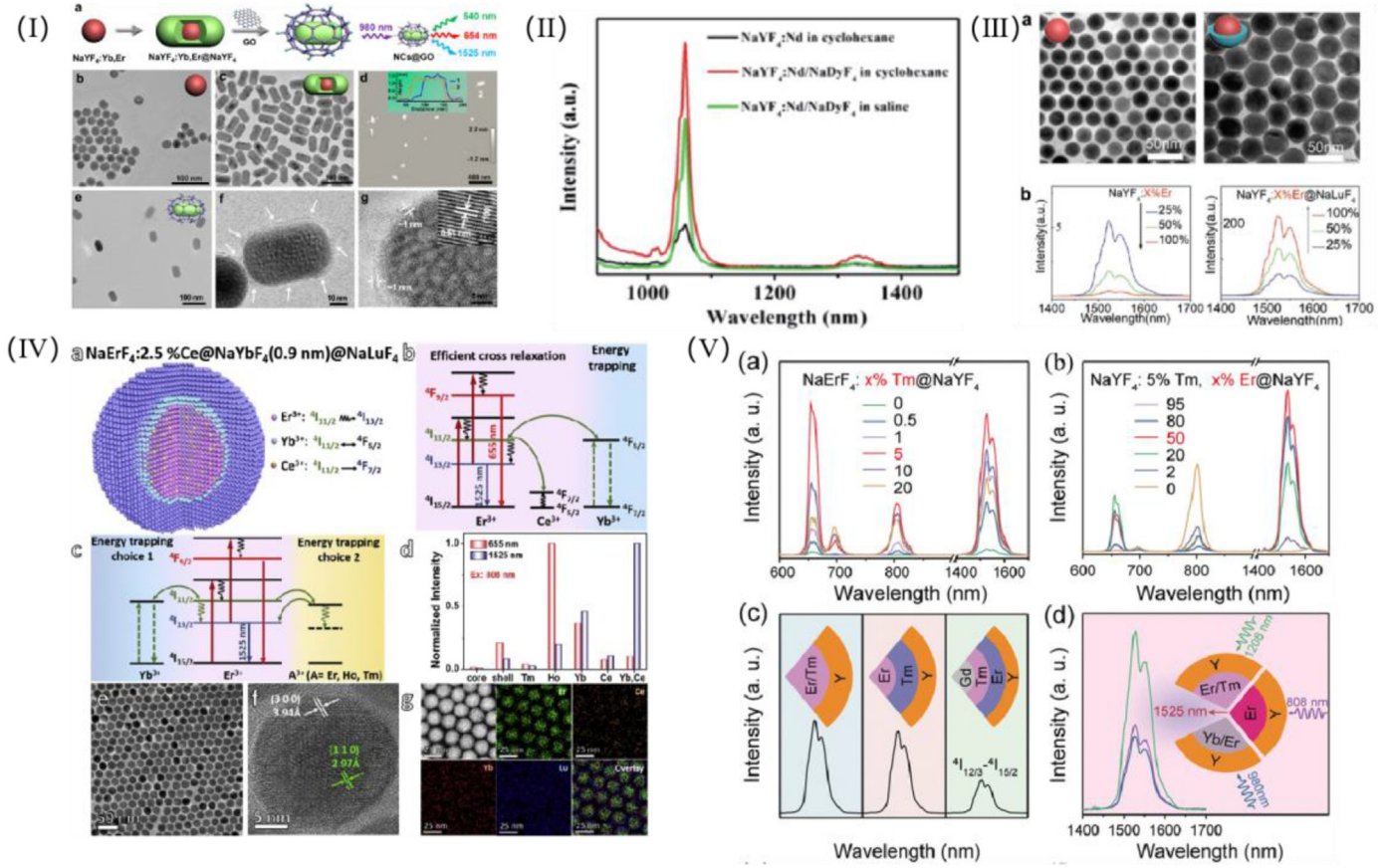

Fig. 3. I) (a) Schematic illustration of the synthesis of NCs@GO. TEM images of (b) core $NaYF_4$:Yb,Er, (c) core-shell $NaYF_4$:Yb,Er@$NaYF_4$, (e) NCs@GO. (d) AFM image of GO, inset: corresponding height image of two marked GO nanosheets. (f) Amplified TEM image of NCs@GO (The arrows indicate GO shell). (g) High-resolution TEM image of NCs@GO. Copyright 2019, Wiley-VCH. II) Luminescence emission spectra of OA-$NaYF_4$:Nd NCs (black), OA-$NaYF_4$:Nd/$NaDyF_4$ NCs (red) and Lipo-$NaYF_4$:Nd/$NaDyF_4$ NCs (green) under excitation of 785 nm. Copyright 2021, Royal Society of Chemistry. III) a) TEM images for nanocrystals of $NaErF_4$ core and $NaErF_4$@$NaLuF_4$ core/shell. b) SWIR luminescence spectra (1400–1700 nm) for $NaYF_4$:X%Er^{3+} core and $NaYF_4$:X%Er^{3+}@$NaLuF_4$ core–shell nanocrystals doped with various Er^{3+} concentrations (x = 25, 50, 100 mol%). Copyright 2018, Wiley-VCH. IV) a) schematic illustration of prepared $NaErF_4$:2.5%Ce@$NaYbF_4$(0.9 nm) @$NaLuF_4$ nanoparticle and b) correspondingly proposed energy diagram showing the UC (655 nm emission) and DC (1525 nm emission) processes under 808 nm light excitation; c) proposed energy diagram showing excitation energy trapping mechanisms of Yb^{3+} ions between Er^{3+} ions, and of A^{3+} (A = Er, Ho, Tm) ions between Er^{3+} ions; d) normalized emission intensities of 655 nm and 1525 nm of $NaErF_4$ core, $NaErF_4$@$NaLuF_4$,$NaErF_4$@$NaAF_4$@$NaLuF_4$(A = Tm-0.4 nm, Ho-0.2 nm, Yb-0.9 nm), $NaErF_4$:2.5%Ce@$NaLuF_4$, and $NaErF_4$:2.5%Ce@$NaYbF_4$(0.9 nm)@$NaLuF_4$ nanoparticles under 808 nm light excitation; e) TEM image, f) High-resolution TEM image, g) HAADF-STEM image, and corresponding elemental maps of Ce, Er, Yb, and Lu of the as-prepared $NaErF_4$:2.5%Ce@$NaYbF_4$(0.9 nm)@$NaLuF_4$ nanoparticles. Copyright 2020, Elsevier. V) a,b) Upconversion and downshifting spectra of $NaYF_4$: x%Tm^{3+},y% Er^{3+}@$NaYF_4$ nanocrystals with different Tm^{3+} and Er^{3+} doping concentrations. The laser power density of 1208 nm laser is 10 Wcm^{-2}. c) The 1525 nm emission of $NaYF_4$:5%Tm^{3+},50%Er^{3+}@$NaYF_4$, $NaErF_4$@$NaYF_4$:20% Tm^{3+}@$NaYF_4$, $NaGdF_4$@$NaYF_4$:10%Tm^{3+}@$NaErF_4$@$NaYF_4$ nanocrystals under 1208 nm excitation. d) Luminescence spectra of $NaYF_4$:5% Tm^{3+},50% Er^{3+}@$NaYF_4$,$NaErF_4$@$NaYF_4$, $NaYF_4$:2%Er^{3+}, 18%Yb^{3+}@$NaYF_4$ nanocrystalsexcited by 1208 nm, 808 nm, and 980 nm lasers, respectively. The laserpower densities are all 10 Wcm^{-2}. Copyright 2019, Wiley-VCH. (For interpretation of the references to colour in this figure legend, the reader is referred to the Web version of this article.)

Drexhage [123]. So far, the metal enhanced fluorescence (MEF) has been mainly used in the preparation of biological probes with high fluorescence intensity, disease detection, DNA testing or other biological applications. Gryczynski found that the SPR effect of metal nanoparticles is closely related to the morphology and size of metal nanoparticles, and pointed out that when the absorption wavelength is greater than the size of nanoparticles, the surface absorbance is only related to the dipole resonance mode [124].

Fluorescence enhancement based on noble metal SPR is a promising method to improve the fluorescence intensity of materials [125,126]. In 2020, Tian's group designed a core-shell structure of nanoparticles $NaYF_4$@SiO_2@Au. With the increase of coated gold nanoparticles, the fluorescence of the material was significantly enhanced. By means of DDA simulation, three layers of LBL gold particles were coated on the surface of the nanomaterial, and the fluorescence intensity of the nanomaterial was increased by up to 7.35 times [96]. Song group used annealing method to compound Ag particles with YVO_4:Yb^{3+},Er^{3+}. By controlling the coupling and effective distance between SPR and excitation light, the fluorescence intensity is finally increased by 30–36 times [97].

The strategy of obtaining enhanced fluorescence emission by designing the structure of noble metal nanoparticles to produce SPR has been widely studied [127]. However, due to the inherent electronic configuration of these metals, they often lack good selectivity. Huang's research group achieved 10 times selective fluorescence enhancement by combining the UV-SPR of cheap non noble metal InNCs with $NaYbF_4$:Tm. This work enriches the basic research of SPR enhanced fluorescence emission [128]. Since the distance between the metal coating and the luminescent particles is a significant factor affecting the SPR effect, this law can also be used for some biological detection [129,130]. Chen's group prepared a novel fluorescent probe for detecting alpha fetoprotein (AFP) by coating $NaYF_4$:Yb,Er, Gd with nano gold. When AFP was added

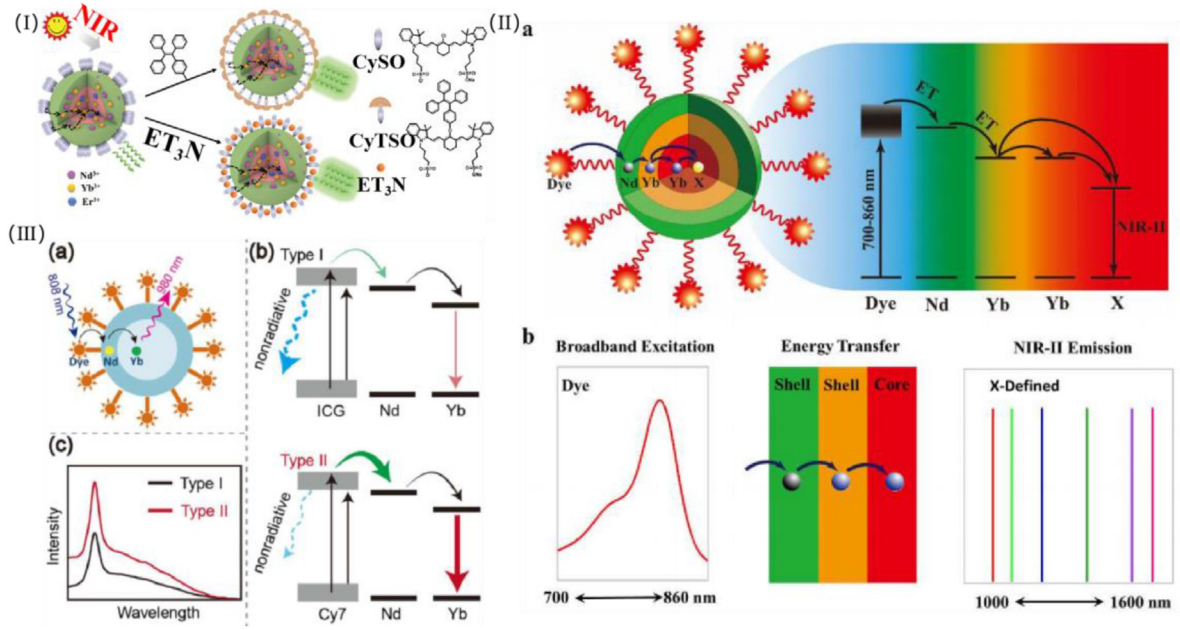

Fig. 4. I) Schematic design and energy transfer in dye-sensitized CS-UCNPs with enhanced upconversion emission under 785 nm excitation. Copyright 2022, Royal Society of Chemistry. II) Schematic illustrations of (a) energy transfer pathway from ICG on the surface of $NaYF_4:Yb^{3+}/X^{3+}@NaYbF_4@NaYF_4:Nd^{3+}$ nanocrystal, to the Nd^{3+} ions in the outer shell, then to the Yb^{3+} in the inner shell, and finally to the Yb^{3+}/X^{3+} (X = null, Er, Ho, Tm, or Pr) in the core, producing large Stokes-shifted NIR-II emissions; (b) the functions of ICG (providing excitation between 700 and 860 nm, 40 μg/mL in DMF), the core/shell/shell structure (spatial isolation of the core from surrounding quenching center, and directing energy transfer to the core), and the activator of varying type (entailing defined narrow band emission in the NIR-II range). Copyright 2016, American Chemical Society. III) (a) The proposed structure of the dye-sensitized core/shell nanoparticles. (b) The energy transfer pathway between dyes and lanthanide ions when using two kinds of dye, marked as Type I and Type II respectively. (c) The schematic spectra of the two types of nanomaterial. Copyright 2018, Royal Society of Chemistry.

to the system, the binding affinity between AFP and anti alpha fetoprotein resulted in the shortening of the distance between gold and $NaYF_4$:Yb,Er, Gd nanoparticles (Fig. 5). The SPR effect of gold nanoparticles enhanced the fluorescence intensity of the system, thus realizing the detection of AFP [98]. In order to achieve efficient SPR fluorescence enhancement in colloids, Song's group increased the fluorescence intensity by 25 times by increasing the thickness of the intermediate layer to 7.5 nm in the Au–Ag nanocage@$NaYF_4$@$NaYF_4$:Yb nanomaterials, which is due to the inhibition of the energy transfer from Er^{3+} to Ag particles and the thermal expansion of Ag particles to Er^{3+} [131]. In addition, the non-metallic SPR can also be used to enhance the fluorescence of nanomaterials [132]. Li synthesized a hybrid material RENPs/WO_{3-x} by using a simple layer method. Under 980 nm excitation, the fluorescence intensity of the material is enhanced by more than 500 times, which is attributed to the strong SPR absorption and thermal effect produced by WO_{3-x} plasma [133].

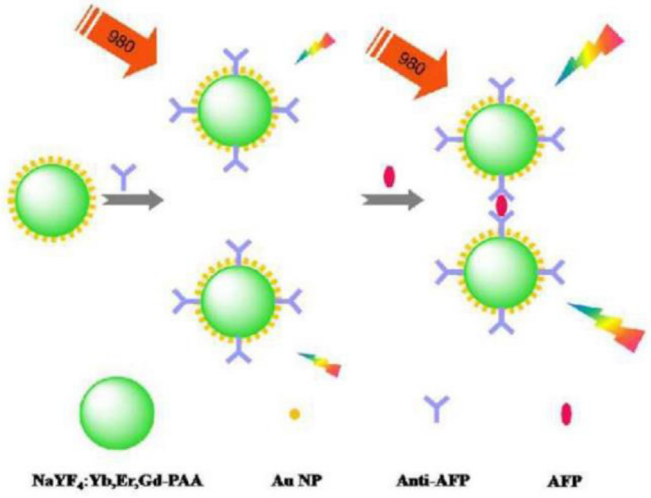

Fig. 5. Schematic illustration of SPR assays based on the gold NPs coated $NaYF_4$:Yb,Er, Gd UCNPs. Copyright 2017, Royal Society of Chemistry. (For interpretation of the references to colour in this figure legend, the reader is referred to the Web version of this article.)

4. Recent application

4.1. NIR-II detection of Tumor

NIR fluorescence imaging technology provides a new noninvasive detection and imaging method for tumor detection and research because of its high sensitivity and high temporal and spatial resolution. It plays an important role in biomedical and clinical diagnosis [134,135]. However, traditional NIR fluorescent contrast agents still face some challenges in vivo, such as shallow tissue penetration and low signal-to-noise ratio. In recent years, the NIR-II lanthanide NPs are considered as a promising biological imaging contrast agent (Table 2). By changing the Ln^{3+} dopant and material structure, the emission wavelength, excitation wavelength and fluorescence lifetime of materials can be accurately controlled, making them an ideal candidate material for various tumor imaging diagnosis [59–61,136]. The development of new high-sensitivity NIR-II lanthanide NPs will be of great significance to achieve efficient early diagnosis of tumor and high-quality monitoring of tumor blood vessels [137]. A pure hexagonal, uniformly sized, strongly NIR–II–emitting polyacrylic acid (PAA) modified nanorods (PAA-NRs) $NaLuF_4$: Gd/Nd has being explored for highly sensitive bioimaging and NIR light-guided tumor detection. The NIR-II emission of this material can be tuned by doping Nd^{3+}, and the emission centers are located at 1056 nm and 1328 nm. The results of animal experiments show that NIR-II optical imaging guided tumor diagnosis has been successfully achieved (Fig. 6I). Notably,

Table 2
Summary of application of lanthanide nanomaterials.

Type of LnNPs	Coating/modifier	Application stage	Bio-application	Sensitizer/activator	Ref.
β-$NaErF_4$:0.5%Tm@$NaLuF_4$	PEG-b-PCL	In vivo	NIR-II imaging of Brain	-/Er^{3+}	[108]
$NaYF_4$:Nd@$NaDyF_4$	phospholipid	In vivo	NIR-II imaging and MRI of HeLa cells	-/Nd^{3+}	[83]
$NaErF_4$:Ce@$NaYbF_4$@$NaLuF_4$	angiopep-2 peptide (ANG)	In vivo	NIR-Guided surgical resection	-/Er^{3+}	[65]
$NaYF_4$:Gd, Yb,Nd,Er,Ce@$NaYF_4$:Nd	PAA	In vivo	Imaging-guided resection surgery of tumor/vascular visualization	Nd^{3+}/Er^{3+}	[104]
$NaYF_4$:Yb/Tm@$NaYF_4$	peptides RGD10-NGR9	In vivo	Tumor (A549 cells)-Targeting Imaging	Yb^{3+}/Tm^{3+}	[106]
$NaYbF_4$:Tm@$NaGdF_4$:Yb	PVP	In vivo	NIR-to-NIR UCL/MRI/CT trimodal imaging probes for tumors	Yb^{3+}/Tm^{3+}	[87]
$NaErF_4$@$NaYF_4$	antibody to the squamous cell carcinoma antigen	In vivo	early-stage squamous non-small-cell lung cancer diagnosis	-/Er^{3+}	[135]
$NaGdF_4$:5%Nd@$NaGdF_4$	an endogenous tripeptide (Glu-Cys-Gly) with two carboxyl groups	In vivo	Inflammation bioimaging	-/Nd^{3+}	[85]
$NaGdF_4$:Nd^{3+}@$NaGdF_4$	–	In vitro	NIR imaging of HeLa cells	-/Nd^{3+}	[86]
$NaGdF_4$: 5% Nd@$NaGdF_4$	DNA and targeting peptides	In vivo	improve the image-guided surgery for metastatic ovarian cancer	-/Nd^{3+}	[139]
$NaYF_4$:5%Nd@$NaGdF_4$	1,2-distearoyl-sn-glycero-3-phosphoethanolamine-N-[methoxy (polyethylene glycol)-2000]	In vivo	multimodal imaging of tumor vasculature	-/Nd^{3+}	[140]
$NaErF_4$@$NaYF_4$	PAA	In vivo	A new NIR-II biological contrast agent	-/Er^{3+}	[141]
CaS:Ce^{3+},Er^{3+}	a layer of amphiphilic phospholipids	In vitro	Detection of biomarker	Ce^{3+}/Er^{3+}	[142]
$NaYbF_4$: 2%Er,2%Ce,10% Zn@$NaYF_4$	anti-PD-L1 (programmed cell death-1 ligand-1) antibody	In vivo	Imaging of PD-L1 in a mouse model of colon cancer	Ce^{3+},Yb^{3+}/Er^{3+}	[134]
$NaErF_4$@$NaYF_4$	anti-SCCA	In vivo	Accurately identify lung squamous carcinoma	-/Er^{3+}	[135]
$NaGdF_4$:Yb/Er/Ce@$NaYF_4$:Nd@$NaGdF_4$	DSPE-PEG-DBCO	In vivo	Real-time, in vivo tumor visualization	Ce^{3+},Yb^{3+}/Er^{3+}	[59]
$NaLuF_4$: Gd/Nd	PAA	In vivo	NIR-II optical imaging-guided small tumor detection	-/Nd^{3+}	[138]
$NaLuF_4$:Yb/Er/Gd/Ce	PAA	In vivo	High sensitivity tiny tumor detection, tumor vessel visualization and brain vessel imaging.	Ce^{3+},Yb^{3+}/Er^{3+}	[143]

small vessels (~105 μm) with high spatial resolution can be clearly detected in vivo [138].

The detection of small tumors in vivo plays a very important role in the early diagnosis of tumors. However, so far, due to the low uptake and easy degradation of macromolecular drugs, the diagnosis of micro tumors (less than 5 mm) is still a great challenge [144]. Recent studies have shown that NIR-II fluorescent lanthanide nanoparticles can be used to accurately identify micro tumors [145]. Zeng's research group designed a lanthanide doped NIR-II fluorescent nanomaterial. By changing the doping concentration of Ce ions, the emission intensity and quantum yield of the nanomaterial at 1525 nm were significantly improved. It is applied to optical guided high-quality and high-resolution tumor angiography to reveal the distribution of blood vessels around the tumor. Moreover, the NIR-II optical guided detection of micro metastases (~4 mm) is also realized (Fig. 6II), which is an important step towards realizing high sensitivity and early diagnosis of tumors [143]. Among various types of tumors, the early detection of liver related tumors is more difficult. Because a large number of intravenous nanoparticles will be captured by the liver, resulting in extremely high fluorescence intensity background signal interference. In view of this problem, Zhang proposed a precise detection method for orthotopic liver tumors based on fluorescence lifetime imaging (Fig. 6III). He constructed the Nd doped nanoparticles with NIR-II luminescence as energy donor and the dye MY-1057 responsive to reactive nitrogen species in tumor microenvironment as energy acceptor. The fluorescence lifetime of the nanoparticles was determined by the number of MY-1057 receptors on the surface, and the fluorescence lifetime was linearly restored in the presence of active nitrogen species in the tumor microenvironment. It is noteworthy that, unlike the fluorescence intensity recovery curve, the fluorescence lifetime recovery curve remains highly consistent at different tissue penetration depths. Therefore, these nanoparticles can quantitatively detect the active nitrogen species in the tumor microenvironment. Compared with fluorescence intensity imaging with low signal-to-noise ratio, fluorescence lifetime imaging can accurately distinguish liver tumors from normal liver tissues, and its results are highly consistent with clinical standard MRI and anatomical results [146].

The current use of existing NIR-II nanomaterials for imaging detection of brain tumors presents several challenges. These include limited imaging depth and spatial resolution, as well as poor blood-brain barrier permeability. These limitations significantly impact the imaging performance of brain tumors and hinder the application of surgical resection. Liu designed a kind of lanthanide doped nanoparticles coated by brain tumor cell membrane for brain tumor imaging and surgical navigation (Fig. 6IV). The coating of brain tumor cell membrane enables the material to have the ability of immune escape, blood-brain barrier crossing and homologous targeting, which are inherited from the brain tumor cells. In addition, compared with indocyanine green, a clinically recognized imaging agent, this material has higher temporal and spatial resolution, higher stability and lower background signal, and can clearly distinguish brain tumor boundaries. With the guidance of NIR-IIb fluorescence, the glioma tissue (size<3 mm, depth>3 mm) could be clearly visualized and completely removed as a proof of concept [147].

Temperature is one of the most basic physiological indicators of organisms. For example, somatic cell can respond to environmental temperature through their own temperature receptors and complete a series of physiological processes. Some diseases show different temperatures from normal tissues due to their abnormal metabolic rates, which makes temperature monitoring important in medical diagnosis and treatment [148,149]. Lanthanide proportional thermometers can calculate and measure temperature changes in tissues or cells in the body based on the intensity ratio of different emission peaks. This can provide a new approach for the diagnosis of diseases such as tumors [150]. When using lanthanide proportional thermometers, the fluorescence emitted can not only discriminate the tumors from healthy tissues, but also monitor the temperature changes in tumor areas in real-time to guide the process of photothermal therapy [151,152]. In addition to the function of temperature measurement, lanthanide nanomaterials can also serve as a

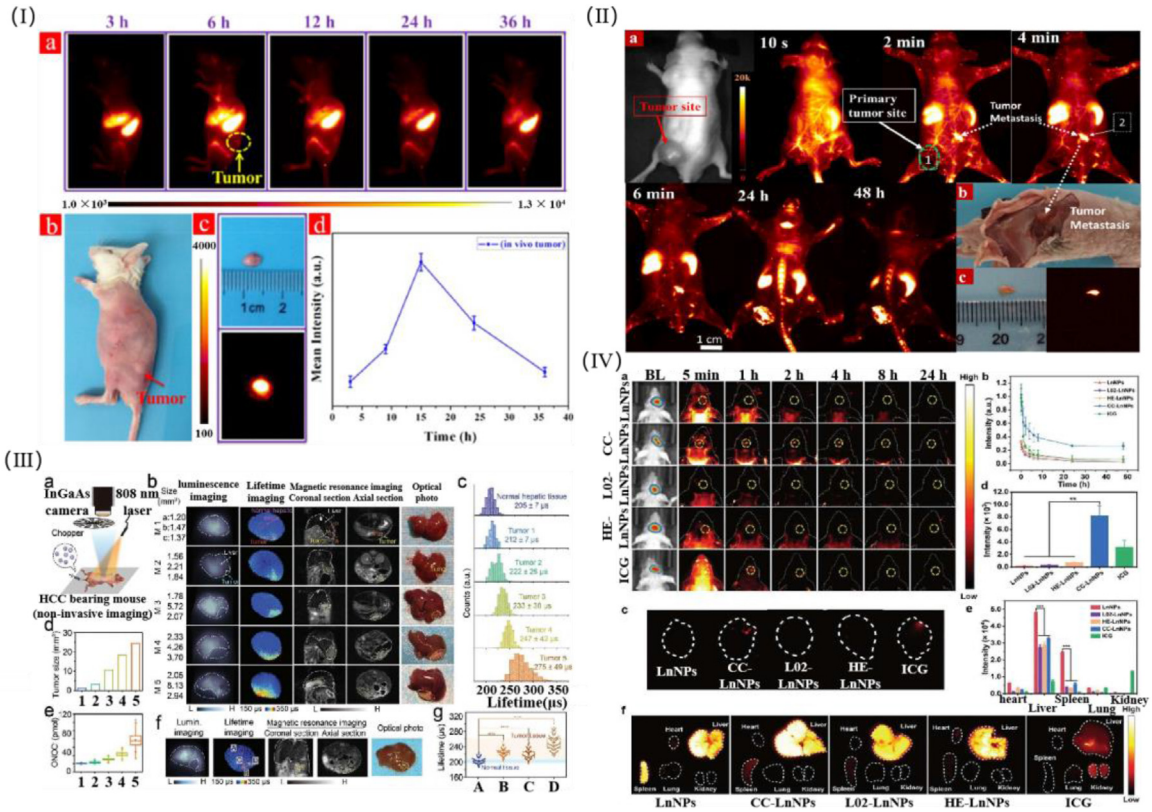

Fig. 6. I) (a) In vivo optical bioimaging of small tumor-bearing mouse after intravenous injection with PAA-NRs at different time intervals; (b) digital photographs of mouse and tumor indicated by red arrow; (c) the corresponding digital photograph of the dissected tumor and ex vivo NIR-II bioimaging; (d) average optical signal intensity in tumor site. Copyright 2019, Elsevier. II) (a) Non-invasive optical imaging-guided tumor metastasis/vessel imaging. Tumor site 1 was the original cultured tumor, tumor site 2 was the metastasis tumor from site 1. (b) In situ digital photograph of the LLC tumor-bearing mouse with skin dissected. (c) Ex vivo NIR-IIb bioimaging (right panel) and the digital photograph (left panel) of the metastasis tumor. Copyright 2016, American Chemical Society. III) In situ HCC tumor detection by noninvasive NIR-II luminescence-lifetime imaging after administration of DSNP@MY-1057-GPC-3 nanosensor. a) Imaging setup for noninvasive lifetime imaging in NIR-II region. b) Noninvasive intensity-based imaging, lifetime-based imaging, and MRI of HCC bearing mice and optical photo of dissected livers. Tumor lesions and normal hepatic tissues are marked as indicated. c) Luminescence lifetime distribution, d) measured size and e) calculated ONOO− amount of Tumors 1–5. f) Noninvasive intensity-based imaging, lifetime-based imaging of a mouse bearing multiple HCC lesions and optical photo of the dissected liver. ROI A: normal hepatic tissue; ROI B–D: tumor lesions distinguished from lifetime imaging. g) Lifetime extracted from ROI A–D of (f). Copyright 2020, Wiley-VCH. IV) a) In vivo fluorescence imaging of tumor-bearing mice treated with LnNPs, CC-LnNPs, L02-LnNPs, HE-LnNPs (200 μL, 5 mg mL^{-1}) and free ICG (200 μL, 0.1 mg mL^{-1}). The fluorescence signals of LnNPs, CC-LnNPs, L02-LnNPs, and HE-LnNPs were collected under 980 nm excitation (112.5 mW cm^{-2}, 300 ms exposure time) with a 1300 nm long-pass (LP) filter. ICG fluorescence signals were collected under 808 nm excitation (75 mW cm^{-2}, 50 ms exposure time) with a 1100 nm LP filter. The first image in each row shows bioluminescence imaging of mice after intraperitoneal injection of D-luciferin sodium salt. b) Quantitative analysis of the fluorescence signals of different nanoparticles and free ICG in the brain tumor region at different time (n = 3). c) Ex vivo images and d) corresponding quantitative fluorescence analysis of brains at 4 h post-injection. e) Quantitative biodistribution of different nanoparticles and free ICG in nude mice determined by the average fluorescence intensity of each organ. f) Ex vivo fluorescence images of major organs dissected from mice injected with different nanoparticles and free ICG at 4 h post-injection. Copyright 2022, Wiley-VCH. (For interpretation of the references to colour in this figure legend, the reader is referred to the Web version of this article.)

sensitive chemical sensor to detect tumor biomarkers, thereby clearly distinguishing the location of tumors. Li has constructed a nanomaterial $NaErF_4$:Ce@$NaYbF_4$@$NaLuF_4$ that can efficiently emit light in the NIR-II region. And further modified its surface with a tumor targeting angiopep-2 peptide, which could target the glioma in a mice model. Finally, They obtained a high tumor-to-background ratio (TBR = 12.5) in the targeted NIR-IIb fluorescence imaging of small orthotopic glioma (size<3 mm, depth>3 mm) through intact skull and scalp [65]. Sialic acid (SA) is a biological molecule that is overexpressed on tumor cell membranes, and increased serum SA concentration has been observed in tumor-bearing patients. The efficient detection of it will help improve the diagnostic ability of tumors. Zheng has designed a series of lanthanide coordination complexes with fluorescence properties as sensors for SA. Among them, TDA−Co−Eu has the highest sensitivity to SA. The deposition of Eu^{3+} on tumor cell membranes has been successfully used to inhibit tumor growth. Therefore, TDA−Co−Eu may be used as an integrated diagnostic and therapeutic reagent for tumors [153].

4.2. Multimode imaging

In the past decade, several technologies have emerged as powerful tools for biomedical research and clinical diagnosis, such as MRI, CT, and ultrasound imaging (USI) [62–64]. Each imaging mode has distinct characteristics in terms of sensitivity, resolution, penetration depth, and cost. However, due to equipment and light source limitations, they will have shortcomings in some aspects, resulting in an inability to provide effective and accurate information about biological structure and physiological processes, hindering clinical diagnosis. Therefore, a noteworthy strategy to improve the quality of biological imaging is to leverage the advantages of various imaging technologies and build a multimodal imaging system to compensate for each other's limitations [154].

NIR-II fluorescence imaging has shown great advantages in the field of biological imaging due to its many characteristics [155]. However, to achieve further breakthroughs in imaging resolution and depth, it is no longer sufficient to rely solely on the design and improvement of the materials themselves [156]. In order to obtain more comprehensive and

high-resolution biological tissue structure information, various imaging methods are demanded to collect as many signals as possible. Therefore, it is urgent to combine NIR-II fluorescence imaging technology with other imaging technologies to form multimode biological imaging in order to improve the quality of bioimaging [157]. High-resolution CT imaging relies on the high X-ray attenuation coefficient of the contrast material, which depends on the atomic coefficient and electron density. Lanthanide nanoparticles have high X-ray absorption capacity in CT imaging due to their atomic coefficient, which is much higher than that of biological tissues [158]. Therefore, the NIR-CT dual-mode imaging with high quality can be achieved based on such materials, providing more accurate information for medical imaging detection [159–161]. The nanoparticles containing Lu^{3+} can be used as an efficient CT imaging contrast agent. Even the Hu value of the $NaLuF_4$ nanoparticles solution with the same concentration can reach 5 times that of standard iodine solution.

MRI is a type of tomography that offers unique advantages over other imaging technologies. While its spatial resolution may be lower than that of CT, MRI is highly flexible and capable of providing a wealth of information [162,163]. When combined with the NIR-II imaging mode, the strengths of both technologies can be leveraged to their fullest potential. It can show the structure and physiological process of biological tissue in more detail [162,164–167]. Among many lanthanide ions, the paramagnetic Gd^{3+} exhibits bright T_1-weighted MRI characteristics due to the presence of seven unpaired 4f electrons. In addition, Gd^{3+} are widely used as sensitizers to activate adjacent Ln^{3+} emitters (Er^{3+}, Ho^{3+}, Tm^{3+} and Nd^{3+}). By doping Gd^{3+} into nanoparticles, the integration of NIR imaging and MRI can be realized. Liu reported the application of bioorthogonal nanoprobes $NaGdF_4$:Yb/Er/Ce@$NaYF_4$:Nd@$NaGdF_4$ with high tumor targeting specificity in NIR imaging and MRI in vivo. Compared with nonbiological orthogonal nanoprobes, these bimodal nanoprobes can enhance NIR-IIb emission by 20 times and MRI signal by 2 times in subcutaneous tumors of mice, and can clearly realize in situ imaging of brain tumors [59]. Multimodal imaging nanomaterials can integrate different imaging functions into a single nanoplatform, providing more comprehensive and accurate information for biological imaging diagnosis. However, it is challenging to design a single type of contrast agent suitable for various imaging modes at the same time. And simply integrating different components into a single matrix can not guarantee the performance of each component [168]. Lanthanide nanomaterials are considered as a promising nanoplatform for multimode imaging [169]. The fluorescence emission intensity of the active core-shell structure nanomaterials $NaYbF_4$:Tm@$NaGdF_4$:Yb-PVP at 800 nm was increased by 7.2 times after plating with $NaGdF_4$:Yb active shell. The nanomaterials have good longitudinal relaxation ($r_1 = 3.58$ L/(mmol s)) and strong X-ray attenuation (58.84 Hu L/g). After intravenous injection of this material in vivo, small tumors were clearly distinguished in T_1-weighted MRI and CT imaging mode, indicating that the modified material can be used as a three modality (NIR/MRI/CT) imaging probe (Fig. 7I-12III) [87].

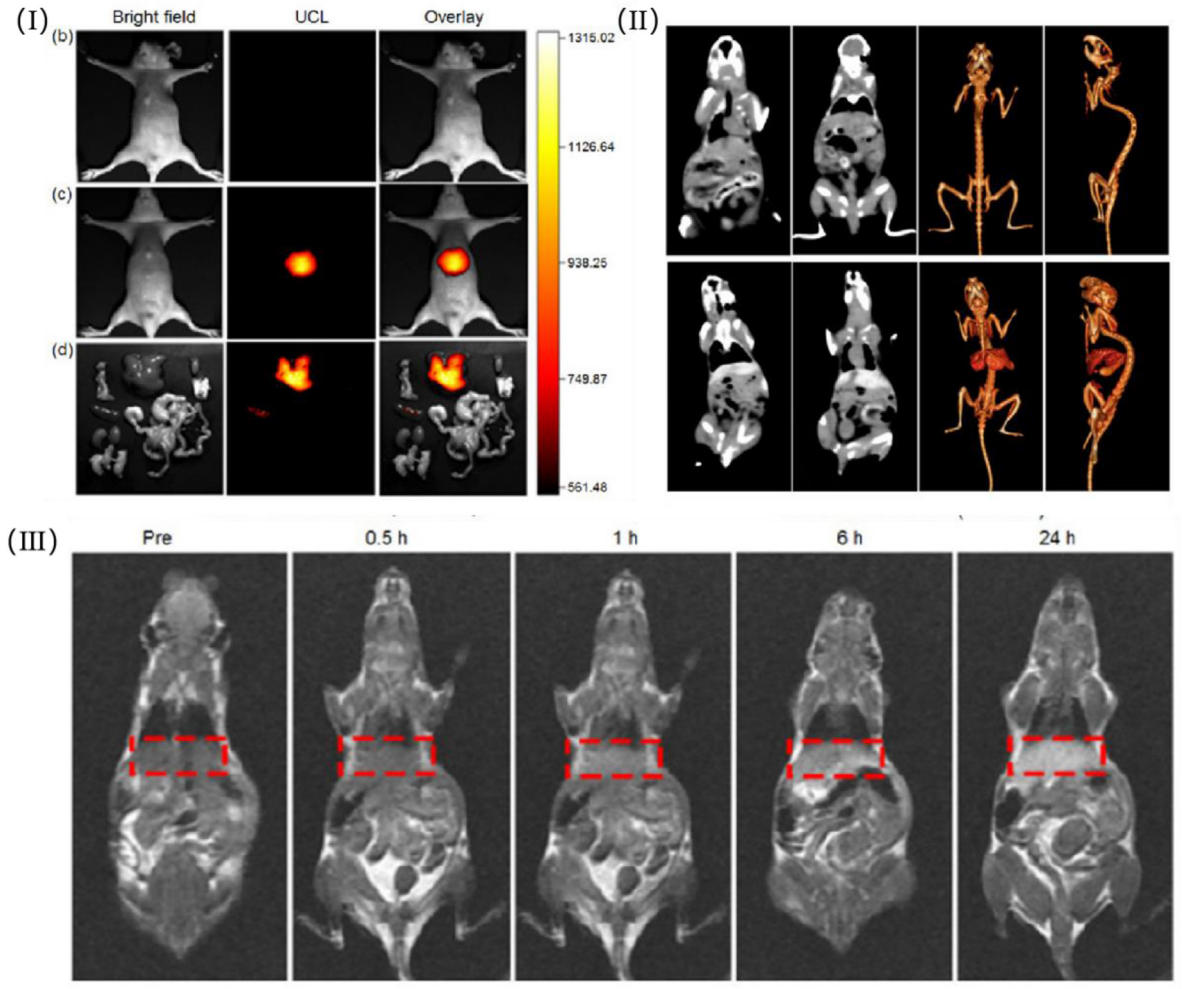

Fig. 7. I) In vivo UCL imaging of mice (power density, 150 mW; irradiation time, 3 s) after intravenous injection (b) without and (c) with $NaYbF_4$:Tm@$NaGdF_4$:Yb-PVP UCNPs. (d) UCL images of dissected mouse and organs, respectively, after intravenous injection with UCM for 24 h II) CT view images of mice in vivo before and 24 h after intravenous injection of $NaYbF_4$:Tm@$NaGdF_4$:Yb-PVP solution. III) T1-weighted MRI before and at different time points (0.5, 1, 6, 24 h) after intravenous injections. Copyright 2017, Elsevier.

4.3. NIR-Guided surgical resection

NIR fluorescence guided surgical resection is a promising development in the treatment of cancer [170]. However, traditional NIR fluorescence contrast agents are unable to clearly delineate the boundaries of tumors due to their low specificity, insufficient light stability and poor tissue penetration depth [171]. Shi et al. designed an improved dual targeting lanthanide NIR nano contrast material by coating polydopamine on the surface of nanomaterials and coupling it with double targeting peptide RGD10-NGR9. The targeting peptide can target integrin αvβ3/αvβ5 and aminopeptidase N receptor on A549 tumor cells. The imaging study of transplanted tumors in BALB/c nude mice shows that the tumors can be distinguished from the surrounding normal tissues by the strong NIR fluorescence of the nano contrast material. This dual targeting nano contrast material has great clinical application potential in NIR fluorescence guided surgery of lung cancer [106]. Accurate surgical resection of tumor plays a vital role in the complete cure of tumor. Clearly defining the tumor edge is very important. Therefore, the development of a high-sensitivity contrast agent to accurately outline the tumor edge is of great significance for accurate and complete resection of the tumor. Zeng's research group has developed a novel nano contrast material $NaYF_4$:Gd/Yb/Er/Nd/Ce@$NaYF_4$, which can significantly improve the NIR-IIb emission above 1500 nm and eliminate the overheating effect. It can easily delineate the edge of the tumor at 24 h after injection. Then, based on NIR-IIb dynamic fluorescence imaging, they completed the resection of the tumor and verified it by the H&E staining analysis (Fig. 8I) [104]. In 2020, Li's research group made new progress in brain glioma surgery guided by NIR fluorescent nano contrast agent. Based on Er^{3+} doped nanoparticles with NIR fluorescence characteristics, they realized the efficient delivery of NIR fluorescent nanomaterials and tumor resection under the guidance of fluorescence imaging by combining the specificity of targeted peptides and the strategy of focused ultrasound to open the blood-brain barrier (Fig. 8II). This also proves the potential of this kind of NIR fluorescent materials in clinical tumor resection [65].

4.4. Phototherapy

Tumor is one of the important diseases threatening human health. Early diagnosis and treatment of tumor is crucial to improving the quality of life and cure rate of patients. However, the existing clinical treatment methods, such as radiotherapy and chemotherapy, often come with significant toxic and side effects, which limit their therapeutic effectiveness. The rapid development of lanthanide nanomaterials has brought about new strategies for tumor treatment that have garnered extensive attention [66–68,172]. Compared with the traditional nanomaterials, multifunctional lanthanide nanomaterials possess unique physical and chemical properties that enable them to realize both the diagnosis and treatment of tumors simultaneously [173–175].

Photodynamic therapy (PDT) is a new developing research field for the treatment of malignant tumors [176–178]. It is a kind of light excited chemotherapy. Firstly, the photosensitizer absorbs the energy of photons and reaches its excited state, and produces some oxidative active molecules. Then the oxidative active molecules make the cells begin to die through a series of reactions [179]. In the past ten years, PDT has made remarkable progress in the application of tumor therapy. It stands out for its effectiveness, safety, low side effects, synergy, repeatability and low cost, adding a new treatment method for intermediate and advanced tumors or the tumors that cannot be treated with traditional therapy [180]. Compared with traditional tumor therapies such as surgery, chemotherapy and radiotherapy, the advantage of PDT is that it can selectively eliminate local primary and recurrent tumors without

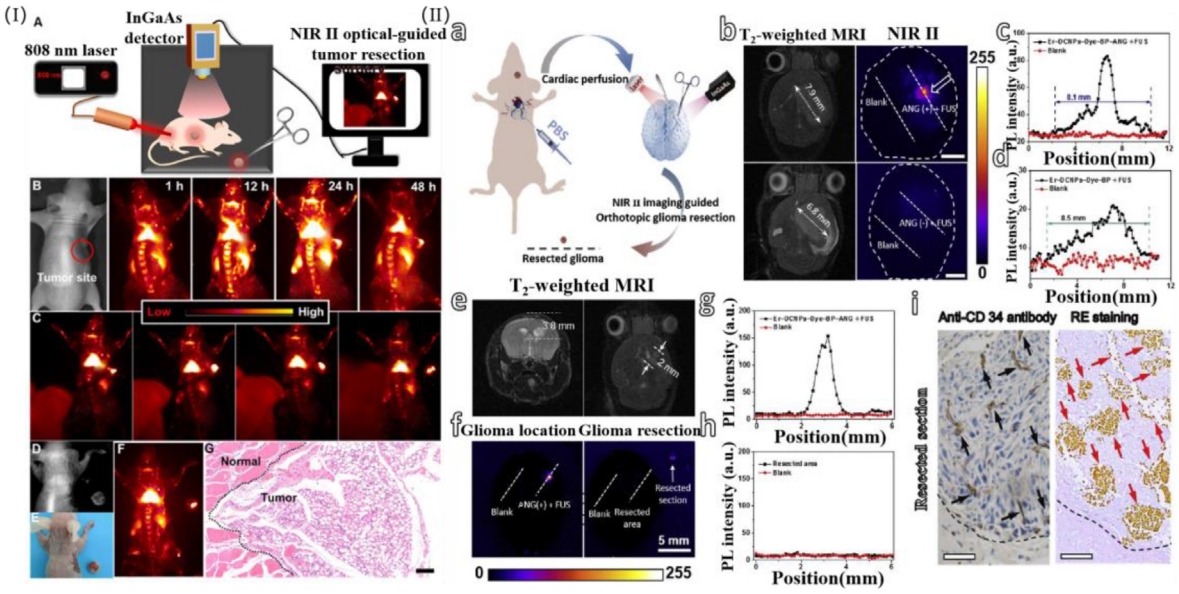

Fig. 8. I) (A) Schematic illustration of the NIR-IIb optical imaging-guided tumor resection. (B) NIR-IIb bioimaging of the colorectal tumor-bearing mouse after intravenously injected with PAA-C/S nanoprobes. (C) Representing images of the dynamic NIR-IIb optical imaging-guided resection of tumor. (D) A bright field image, (E) digital photograph and (F) NIR-IIb imaging of the colorectal tumor-bearing mouse and the resected tumor. (G) H&E analysis of the resected tumor, the margin of the normal tissue and tumor was marked by the black dashed line. Copyright 2020, National Center for Biotechnology Information. II) a) Schematic illustration of NIR IIb fluorescence imaging guided resection of deep-seated and small-sized orthotopic glioma; b) T2-weighted MRI images of large sized glioma (left), and NIR IIb fluorescence images of the resected brain after cardiac perfusion (right); c-d) the corresponding tumor diameter measured from the NIR IIb fluorescence intensity of images acquired at 25 min post injection of nanoprobes and FUS treatment; e) preoperative T2-weighted MRI diagnosis of small deep-seated orthotopic glioma 2 mm in diameter; f) NIR IIb fluorescence images of resected brain, after the mice were intravenously injected with Er-DCNPs-Dye-BP-ANG, treated with focused ultrasound, and subjected to cardiac perfusion (scale bar: 5 mm); g-h) the corresponding NIR IIb fluorescence intensity of the glioma area before and after resection; i) immunohistochemical assay of blood vessels and Arsenazo III staining of rare earth ions in the resected tumor tissue, with the black and red arrows indicating the capillaries and rare-earth ions (scale bar: 50 μm). Copyright 2019, Elsevier. (For interpretation of the references to colour in this figure legend, the reader is referred to the Web version of this article.)

damaging normal tissues [181]. The excitation light source used for PDT is preferably in the NIR band and is located near the photosensitizer absorption peak at the same time. The selection principle of photosensitizer is that it has no side effects on the body [182]. Second, it is selectively ingested by tumors and can be quickly excreted by normal tissues. Third, it has strong photosensitivity, long service life and high yield of reactive oxygen species. At present, the PDT treatment strategy based on lanthanide nano materials can give full play to the imaging advantages of lanthanide materials and the therapeutic ability of photosensitizers at the same time, which has made significant application progress in imaging guided PDT treatment [183,184]. Yan constructed Er^{3+}-doped nanoparticles, whose luminescence overlapped well with the absorption of Zr based porphyrin MOF, effectively transferring energy from NaLnF4 to MOF shell to generate $^1O_2$. At lower excitation power, the position and distribution of heterostructures can be tracked by NIR II imaging. And antiprogrammed death-ligand 1 (α-PD-L1) immunotherapy was introduced synergistically to improve antitumor immunity efficacy. The combined use of $NaLnF_4$@MOF and α-PD-L1 can not only inhibit the primary tumor, but also inhibit the distal one, with an effective tumor inhibition rate of 95% (Fig. 9I) [185].

Photothermal therapy (PTT) is a promising method for treating tumors that has gained significant attention in recent years. This novel approach has great potential for clinical application due to its low toxicity and lack of drug resistance. Tumor cells become fragile at 42–45 °C and start apoptosis and necrosis. This process is called thermal ablation. PTT uses photothermal conversion agents (PTAs) to obtain energy from NIR light and convert it into heat to increase the temperature of the surrounding environment of the tumor, thereby causing tumor cell death [186,187]. Combining PTAs with lanthanide materials can realize the synergistic effect of NIR fluorescence imaging localization and tumor photothermal therapy [188–190]. Chen invented a lanthanide based therapeutic agent, Prussian blue (PB) coating $NaErF_4$@$NaYF_4$@$NaNdF_4$ core/shell/shell nanocrystals encapsulated in phospholipid polyethylene glycol micelles (PEG-CSS@PB). The Er^{3+} rich core nanocrystals ($NaErF_4$) can emit NIR-IIb light (1525 nm) that can penetrate deep biological tissues under 980 nm light excitation, so it can perform high-resolution optical imaging on blood vessels and tumors. The introduction of high concentration neodymium (Nd^{3+}) in the outer layer $NaNdF_4$ maximizes the cross relaxation process and can efficiently convert the absorbed NIR light (similar to 808 nm) into heat, thus providing the ability of photothermal therapy. Importantly, the coated Prussian blue (PB) increased the light absorption by about 10 times compared with the composite without PB, and thus had a high photothermal conversion efficiency of 50.5%. This is comparable to the performance of gold nanorods. PTT treatment experiments were completed in BALB/c mice. Compared with untreated tumors, the size of tumors irradiated by NIR light was reduced by about 12 times (Fig. 9II) [191]. Wang developed a new DNA-mediated lanthanide material-gold nanoparticle hybrid hydrogel. An ultrastrong photothermal effect was observed due to the confined and concentrated environment caused by the interaction between adjacent DNA strands and the NPs. The photothermal efficiency of 42.7% was achieved in the hydrogel, which was superior to the original inorganic particles. After direct injection of hydrogel around the tumor and treatment with 808 nm laser irradiation, the tumor was eradicated without recurrence. At the same time, local treatment has no side effects on normal tissues [192].

When using lanthanide nanomaterials for phototherapy, simultaneous treatment and fluorescence tracing can pose significant challenges for practical applications. For instance, if lanthanide nanomaterials are used for tumor treatment but have not yet been delivered to the tumor site, stimulating them for tracing purposes can result in unwanted photothermal or photodynamic effects, which can harm normal tissues. To address this issue, Vetrone proposed a decoupled RENPs material that can be orthogonally excited at 980 and 806 nm, resulting in conversion and downshifting emissions, respectively. The conversion emitting light can stimulate photosensitizers to produce singlet oxygen to induce therapeutic effects. And the downshifting emitting light can be used as a non therapeutic optical tracer and nano thermometer. This strategy utilizes the advantages of conversion and downshifting respectively, achieving a reasonable separation between treatment and diagnosis in a most direct and effective way [193]. Another method to avoid the harmful effect of photodamage caused by the "always on" UV-blue light during diagnosis is to design a nanostructured $NaErF_4$@$NaYF_4$@-$NaYbF_4$:0.5%Tm@$NaYF_4$. It undergoes monochromatic red emission when excited at 800 nm, and strong ultraviolet and blue emissions in

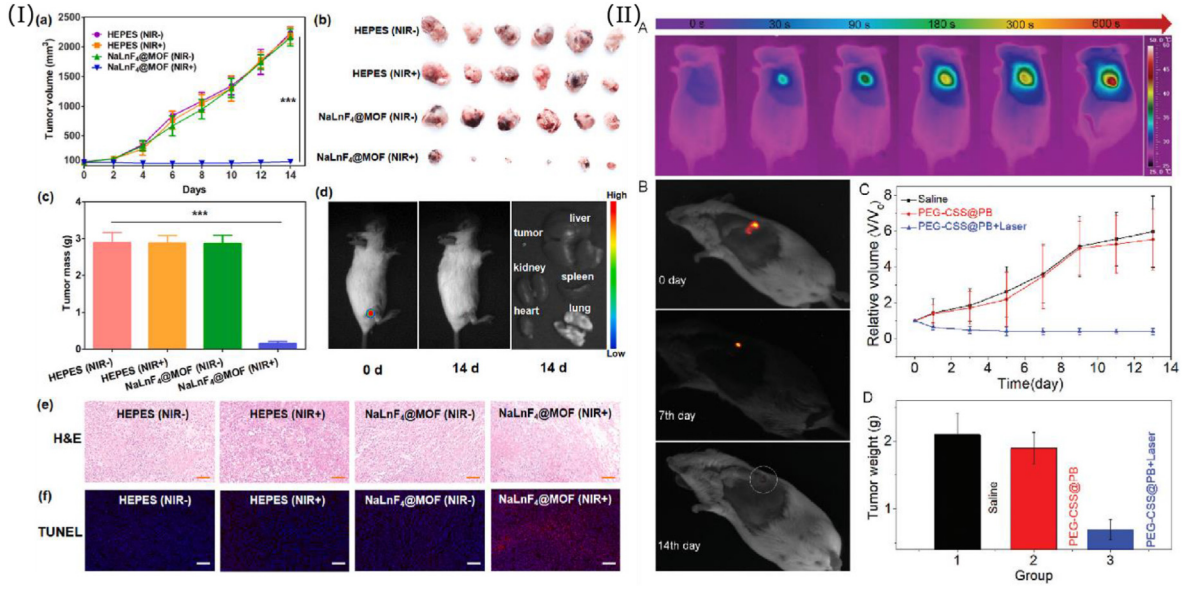

Fig. 9. I) (a) Tumor growth via different treatments. (b) The photos and (c) mass of excised tumor after 14 days post-injection. (d) NIR-II images of tumor-bearing mice and excised organs after PDT. (e) H&E-stained images and (f) TUNEL-stained images of tumors slices for the different groups. Scale bars: 100 μm. Copyright 2022, Elsevier. II) (A) Thermographic images of the tumor-bearing mouse during PTT treatment. (B) Monitoring the tumor treatment outcome through NIR II imaging, which was recorded at 0, 7, and 14 days post photothermal treatment. (C and D) The average tumor volume and weight in three groups of BALB/c mice, including two control groups (intratumorally injected with saline or a PEG-CSS@PB solution) and the PTT-treated group (both with the PEG-CSS@PB nanocomposite and 808 nm laser irradiation). All of the PTT treatment groups utilized an 808 nm light dose of 1 W cm^{-2} for 10 min. Copyright 2019, Royal Society of Chemistry.

addition to red emission when excited at ~980 nm, which guarantees the UV-blue emission coming solely from the UC emission of Tm^{3+}. This strategy offers an alternative strategy for imaging guided "off-on" phototherapy [194].

There is another tumor treatment method based on lanthanide materials. In this method, a core-shell nanoparticle $NaYF_4$:Yb/Tm@$NaYF_4$:Nd with up conversion and downshifting emission was first constructed, and the surface was modified with SO_2 gas prodrug molecule ATD and NIR-II organic dye molecule IR-808. The up-conversion luminescence of this nanoparticle is enhanced by 28 times, which can effectively activate ATD molecules to achieve the on-demand release of SO_2 gas, while its down-conversion luminescence was enhanced by 5 times, which can be used for NIR-II fluorescence imaging of orthotopic glioblastoma. Li further explored the killing mechanism of SO_2 gas released in response to light on tumor. The results showed that SO_2 gas could induce apoptotic autophagy of tumor cells by down regulating p62 protein expression and up regulating the ratio of LC3-II/LC3-I, and finally inhibit the tumor growth [195].

4.5. Drug carrier

With the continuous development of nanotechnology and pharmaceutics, lanthanide nanomaterials as a new drug delivery carrier have attracted widespread attention of researchers due to their non-toxic, excellent optical properties, good biocompatibility and other advantages [196]. However, as lanthanide nanomaterials are typically solid structures without microcavities or mesoporous structures to carry or load functional molecules, the main approach to achieving multifunctional applications including drug release is to combine lanthanide nanomaterials with other matrix materials that possess mesoporous microcavity structures. This approach has garnered widespread attention from researchers [197]. Chen et al. developed a multifunctional lanthanide nano material with hollow core-shell structure. The material consists of the β-$NaLuF_4$:Gd/Yb/Er nanoparticles core and porous silica shell. The introduction of phenyl skeleton and the design of hollow core-shell structure are conducive to the loading of photosensitizer, reducing the agglomeration of photosensitizer, and shorten the distance between photosensitizer and lanthanide nanoparticles. Using this material to load photosensitizer monocarboxy phthalocyanine zinc, the loading amount is 7.7 wt% and the energy transfer efficiency is as high as 98%. Under 980 nm laser irradiation, the lanthanide nanoparticles can sensitize photosensitizers to produce singlet oxygen to enable photodynamic treatment of human lung cancer cells. The effect is significantly better than that of common core-shell drug carrier materials or single silica shell materials [198].

In order to further improve the efficiency of tumor treatment, it is necessary to help the loaded drugs to be accurately delivered to tumor and other focal tissues and completely released. However, the current situation is that most loaded drugs are gradually leaked or decomposed during delivery, and only a very small amount of loaded drugs can be released to the target area for therapeutic use [199]. A clever strategy to solve this problem is to control the release of drugs and build a nanocarriers that can release loaded drugs only under the stimulation of pH, NIR light or other conditions. Lanthanide nanomaterials have been gradually developed for this strategy because of their high photosensitivity, easy customization of structure, good stability and large loading rate [69,70].

The NIR nano core-shell structure material $NaYF_4$:Yb/Tm@SiO_2-doxorubicin (Dox)/curcumin (Cur)-chitosan (CS)/2-Octen-1-ylsuccinic anhydride (OSA) designed by Liu's research group, whose CS/OSA responds to a low pH environment to release cancer drugs, including Dox and Cur for chemotherapy through breaking a free carboxyl group. The results show that this nano material could continuously release Dox and Cur at a pH value of 6.5 within 6 h after the excitation of a 980 nm-wavelength CW laser (Fig. 10I) [200]. Lv combined hydrophobic lanthanide nanomaterials with biocompatible mPEG-PLGA to design a pH sensitive degradable nanoprobe for NIR-IIi imaging guided tumor chemotherapy. The degradable nanoprobe increased the imaging sensitivity, allowed the slow release of internal anti-tumor drugs, and reduced the loss of drugs during the delivery process. After hydrolysis, the probe can discharge about 6 nm ultra-small lanthanide nanoparticles, reducing the enrichment of inorganic materials in vivo [201]. The use of NIR light responsive drug loaded nanoparticles for controlled release can not only prevent the leakage of drugs before delivery to the target location, but also increase the light control depth and avoid local overheating of tissues [202–205].

A strategy based on ultra-small lanthanide nanoparticles (~10 nm) is to coat mesoporous SiO_2 on the surface of nanoparticles to load tumor chemotherapy drug DOX, and then connect ruthenium as a molecular valve on its surface. When excited at 808 nm, the cleavage of ruthenium and uncaping of the pores will be triggered to release DOX for tumor treatment (Fig. 10II) [206]. Through other target response sources, Zhang developed an intelligent manganese dioxide based lanthanide nanotherapy platform ErNPs@MnO_2-siS100A4-RGD. It has the ability to respond to the tumor microenvironment due to the presence of MnO_2. MnO_2 can be degraded by glutathione (GSH) in the tumor area, release siRNA and generate Mn^{2+} at the same time, so as to achieve precise gene therapy and a Fenton-like reaction-mediated chemokinetic therapy (CDT) for malignant triple negative breast cancer (TNBC) (Fig. 10III). The results of in vitro and in vivo experiments showed that the smart nanoplatform had high siRNA delivery efficiency and GSH-responsive siRNA releasing ability. Compared with individual gene therapy, GSH-depletion-enhanced CDT effect further reinforced the TNBC inhibition [207].

5. Conclusion and outlook

In recent years, NIR fluorescence imaging has shown great potential in various fields due to its high sensitivity, high signal-to-noise ratio, and deep tissue penetration ability. This imaging technique has been widely used in tumor diagnosis, biological small molecule detection, biosensor development, immune analysis, and anti-counterfeiting. During the development of NIR fluorescent probes, lanthanide nanomaterials have garnered significant attention due to their strong optical and chemical stability, narrow emission half peak width (10–20 nm), tunable emission wavelength, and fluorescence lifetime. A variety of lanthanide nanomaterials with different doping ion ratios, shell structures, and modification methods have been developed, which not only enhances their luminous efficiency but also expands their potential applications in the biomedical field. However, despite these advancements, there are still some challenges that need to be addressed before these materials can be applied clinically.

(1) Further improvement of the fluorescence intensity of lanthanide nanomaterials

The further improvement of the fluorescence intensity of lanthanide nanomaterials will determine the possibility of future clinical applications. The lanthanide nanomaterials with high fluorescence performance can not only improve the penetration depth of biological tissues, but also minimize the power of excitation light and the amount of material used on the premise of ensuring the imaging quality, so as to reduce the damage to organisms. However, although some strategies (including: coating, dye sensitization, surface plasma enhancement, doping and adjusting the size and morphology) have been used to improve the fluorescence performance of materials, the improvement degree is limited. It can only play some roles in vitro or in mice, and it is still far from clinical application. Therefore, in order to obtain lanthanide nanomaterials with high fluorescence performance that can meet the clinical needs, it is necessary to further explore and develop new strategies to greatly improve the fluorescence performance. A promising strategy is to search for chemically stable host materials with lower

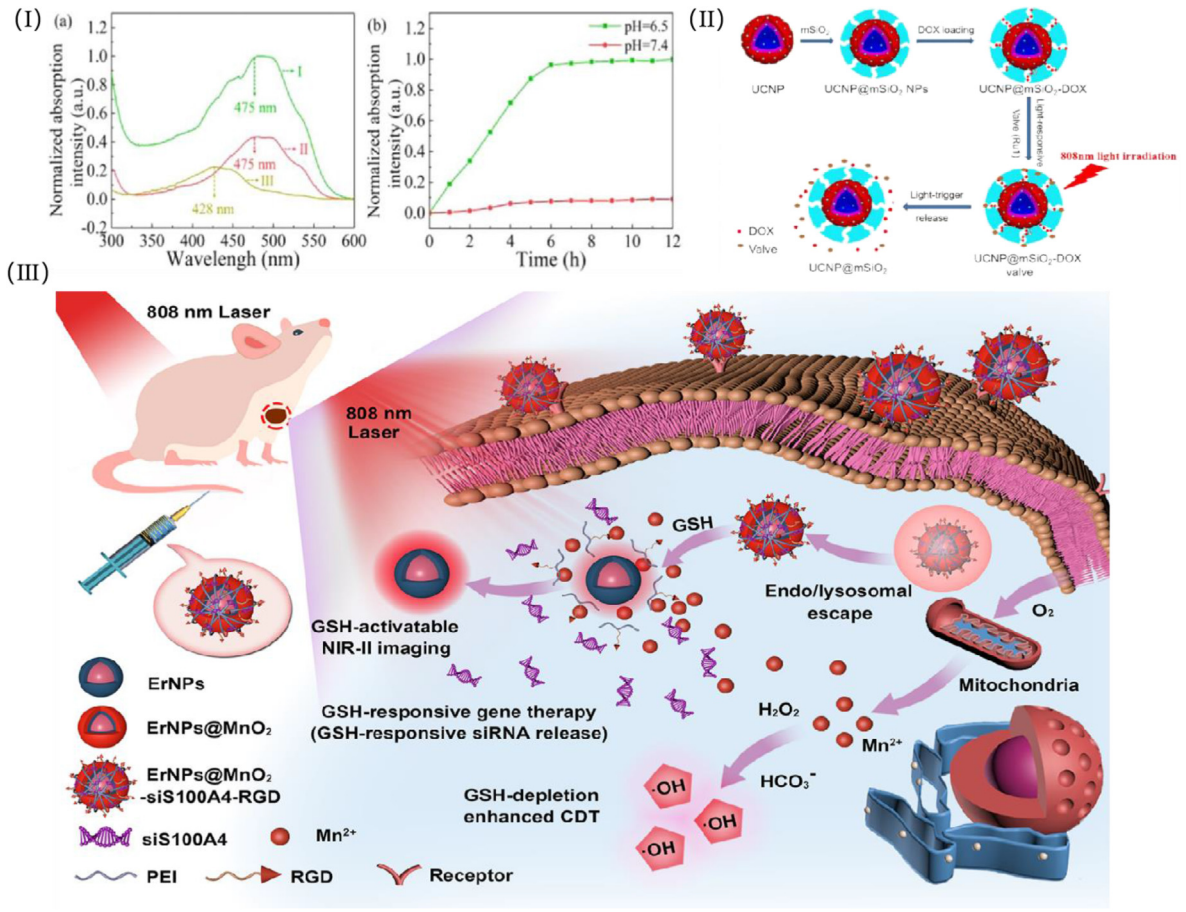

Fig. 10. I) Measurements of the drug release from the $NaYF_4$:Yb/Tm@SiO_2-Dox/Cur-CS/OSA nanoparticles. (a) Normalized absorption spectra of Dox and Cur drugs released from the $NaYF_4$:Yb/Tm@SiO_2-Dox/Cur-CS/OSA (I), $NaYF_4$:Yb/Tm@SiO_2-Dox-CS/OSA (II), and $NaYF_4$:Yb/Tm@SiO_2-Cur-CS/OSA (III) with pH = 6.5. (b) Normalized absorption intensities of Dox and Cur drugs released from the $NaYF_4$:Yb/Tm@SiO_2-Dox/Cur-CS/OSA nanoparticles as a function of time with pH = 6.5 and pH = 7.4. II) Schematic illustration of functionalization of $NaGdF_4$:Yb,Tm,Ca@$NaYbF_4$:Ca@$NaNdF_4$:Gd, Ca UCNPs with mesoporous silica and DOX for chemo-drug loading and release. Copyright 2021, IOPscience; Copyright 2016, American Chemical Society. III) Schematic Illustration of GSH Stimuli-Responsive Lanthanide-Doped NIR-II Luminescent Nanoprobes for TNBC Precise Gene Therapy in Synergism with CDT. Copyright 2021, American Chemical Society.

phonon energy, while assisting in doping with foreign ions to disrupt the lattice symmetry of Ln^{3+} in the NPs host lattice, thereby relieving the electric dipole transition limitation in the f configuration and improving the fluorescence intensity of lanthanide nanomaterials. Another strategy is to enhance the fluorescence lifetime of lanthanide nanomaterials under the current bottleneck of their fluorescence intensity. Because this strategy avoids signal loss and distortion issues that occur during intensity based imaging in deep tissues, and is not affected by biological tissue scattering. In future research, there is still much work to be done to explore more preferred strategies.

(2) Exploration of new strategies for biocompatibility modification of lanthanide nanomaterials

Before applying the material to the living body, it must be ensured that it has good biocompatibility, because this is the guarantee that it can flow through the biological vein to the target area for fluorescence imaging diagnosis and will not produce toxic and side effects on the organism. Although numerous studies have shown that lanthanide nanomaterials have good biocompatibility and no significant toxicity in animal models, their potential long-term toxicity should be systematically and rigorously evaluated in the future, including water solubility, cytotoxicity, blood toxicity and where they can be discharged from the body. Scientists now use various modifiers and modification methods to functionalize or coat NPs to improve their water solubility and biocompatibility, such as PAA, PVP, PEI, SiO_2, PEG, and so on. However, this strategy will inevitably affect the fluorescence intensity of the material and reduce its quantum yield. Therefore, it is of great significance to explore a method that can not only maintain the fluorescence performance but also improve the biocompatibility of lanthanide nanomaterials. More importantly, given the dose-dependent toxicity of lanthanide nanomaterials, further research is needed on their safe dosage to guide the in vivo applications.

(3) The development direction of tumor application

Lanthanide nanomaterials hold great promise for application in tumors, and we believe that their potential can be further developed in the following directions: 1. Integrating multimodal imaging and therapeutic functions into a single nano platform to construct the stimulus responsive lanthanide nanomaterial therapeutic agents. 2. Development of NIR II-NIR II lanthanide nanomaterials with lower tissue self-fluorescence interference and scattering (e.g. the $NaErF_4$:2%Ho@$NaYF_4$ lanthanide nanomaterials with both excitation (1530 nm) and emission (1180 nm) located in the NIR-II window). In addition, the water absorption window (1400–1500 nm) located in the NIR II can also be utilized to attenuate the scattering photons with a long optical path and thus restrain the image background [208]. 3. Develop matching optical medical equipment, such as minimally invasive stimulation fibers, detectors with higher quantum efficiency in the NIR region, and so on. 4. Design lanthanide

nanomaterials with stronger targeted binding properties for specific tumors. Overall, we believe that these developments will further enhance the potential of lanthanide nanomaterials for tumor imaging and therapy.

Declaration of competing interest

The authors declare that they have no known competing financial interests or personal relationships that could have appeared to influence the work reported in this paper.

Data availability

No data was used for the research described in the article.

Acknowledgements

The author(s) disclosed receipt of the following financial support for the research, authorship, and/or publication of this article: Natural Science Basic Research Plan in Shaanxi Province of China (No.2022JQ544), "From 0 to 1″ Original Innovation Project of the Basic Frontier Scientific Research Program of the Chinese Academy of Sciences (29J20-015-III) and Chinese Academy of Sciences's 100 Talents Project: Research on Task oriented Functional Brain Development of Infants (29J20-052-III).

References

[1] U. Cho, J.K. Chen, Lanthanide-based optical probes of biological systems, Cell Chem Biol 27 (8) (2020) 921–936.
[2] P. Pei, Y. Chen, C.X. Sun, Y. Fan, Y.M. Yang, X. Liu, L.F. Lu, M.Y. Zhao, H.X. Zhang, D.Y. Zhao, X.G. Liu, F. Zhang, X-ray-activated persistent luminescence nanomaterials for NIR-II imaging, Nat. Nanotechnol. 16 (9) (2021) 1011–1018.
[3] H.X. Zhang, M.Y. Zhao, I.M. Abraham, F. Zhang, Super-resolution imaging with lanthanide luminescent nanocrystals: progress and prospect, Front. Bioeng. Biotechnol. 9 (2021), 692075.
[4] Y.H. Zhang, X. Ma, H.F. Chau, W. Thor, L.J. Jiang, S. Zha, W.Y. Fok, H.N. Mak, J.H. Zhang, J. Cai, C.F. Ng, H.G. Li, D. Parker, L. Li, G.L. Law, K.L. Wong, Lanthanide-cyclen-camptothecin nanocomposites for cancer theranostics guided by near-infrared and magnetic resonance imaging, ACS Appl. Nano Mater. 4 (1) (2021) 271–278.
[5] X.Q. Ge, Z.M. Song, L.N. Sun, Y.F. Yang, L.Y. Shi, R. Si, W. Ren, X. Qiu, H.F. Wang, Lanthanide (Gd^{3+} and Yb^{3+}) functionalized gold nanoparticles for in vivo imaging and therapy, Biomaterials 108 (2016) 35–43.
[6] M.J. Neufeld, H. Winter, M.R. Landry, A.M. Goforth, S. Khan, G. Pratx, C. Sun, Lanthanide metal-organic frameworks for multispectral radioluminescent imaging, Acs Appl Mater Inter 12 (24) (2020) 26943–26954.
[7] B.L. Ma, X.J. Zhai, G.P. Du, J. Zhou, Orthogonal shortwave infrared emission based on rare earth nanoparticles for interference-free logical codes and bio-imaging, Chem. Sci. 10 (11) (2019) 3281–3288.
[8] S. Plunkett, M. El Khatib, I. Sencan, J.E. Porter, A.T.N. Kumar, J.E. Collins, S. Sakadzic, S.A. Vinogradov, In vivo deep-tissue microscopy with UCNP/Janus-dendrimers as imaging probes: resolution at depth and feasibility of ratiometric sensing, Nanoscale 12 (4) (2020) 2657–2672.
[9] R.R. Tian, S. Zhao, G.F. Liu, H.D. Chen, L.N. Ma, H.P. You, C.M. Liu, Z.X. Wang, Construction of lanthanide-doped upconversion nanoparticle-Uelx Europaeus Agglutinin-I bioconjugates with brightness red emission for ultrasensitive in vivo imaging of colorectal tumor, Biomaterials 212 (2019) 64–72.
[10] Y.H. Wang, S.Y. Song, S.T. Zhang, H.J. Zhang, Stimuli-responsive nanotheranostics based on lanthanide-doped upconversion nanoparticles for cancer imaging and therapy: current advances and future challenges, Nano Today 25 (2019) 38–67.
[11] X.Q. Ge, R.Y. Wei, L.N. Sun, Lanthanide nanoparticles with efficient near-infrared-II emission for biological applications, J. Mater. Chem. B 8 (45) (2020) 10257–10270.
[12] G.F. Liang, H.J. Wang, H. Shi, H.T. Wang, M.X. Zhu, A.H. Jing, J.H. Li, G.D. Li, Recent progress in the development of upconversion nanomaterials in bioimaging and disease treatment, J. Nanobiotechnol. 18 (1) (2020) 154.
[13] M.Y. Zhao, B.H. Li, P.Y. Wang, L.F. Lu, Z.C. Zhang, L. Liu, S.F. Wang, D.D. Li, R. Wang, F. Zhang, Supramolecularly engineered NIR-II and upconversion nanoparticles in vivo assembly and disassembly to improve bioimaging, Adv Mater 30 (52) (2018), 1804982.
[14] Y.D. Bai, Y.M. Li, R. Wang, Y.M. Li, Low toxicity, high resolution, and red tissue imaging in the vivo of Yb/Tm/GZO@SiO2 core-shell upconversion nanoparticles, ACS Omega 5 (10) (2020) 5346–5355.
[15] L.Y. Zeng, D. Wu, Y. Tian, Y.W. Pan, A.G. Wu, J.C. Zhang, G.M. Lu, Recent progress in 808 nm excited upconversion nanomaterials as multifunctional nanoprobes for visualized theranostics in cancers, Curr. Med. Chem. 25 (25) (2018) 2954–2969.
[16] D. Kim, N. Lee, Y.I. Park, T. Hyeon, Recent advances in inorganic nanoparticle-based NIR luminescence imaging: semiconductor nanoparticles and lanthanide nanoparticles, Bioconjugate Chem. 28 (1) (2017) 115–123.
[17] I. Martinic, S.V. Eliseeva, S. Petoud, Near-infrared emitting probes for biological imaging: organic fluorophores, quantum dots, fluorescent proteins, lanthanide(III) complexes and nanomaterials, J. Lumin. 189 (2017) 19–43.
[18] C. Cai, X. Li, Y. Wang, M.X. Liu, X.Y. Shi, J.D. Xia, M.W. Shen, Polydopamine-coated gold core/hollow mesoporous silica shell particles as a nanoplatform for multimode imaging and photothermal therapy of tumors, Chem Eng J 362 (2019) 842–850.
[19] O.R. Taratula, O. Taratula, X.J. Han, Y. Jahangiri, Y. Tomozawa, M. Horikawa, B. Uchida, H.A. Albarqi, C. Schumann, S. Bracha, T. Korzun, K. Farsad, Transarterial delivery of a biodegradable single-agent theranostic nanoprobe for liver tumor imaging and combinatorial phototherapy, J. Vasc. Intervent. Radiol. 30 (9) (2019) 1480–1486.
[20] Y.L. Zhou, J. Zhou, F. Wang, H.F. Yang, Polydopamine-based functional composite particles for tumor cell targeting and dual-mode cellular imaging, Talanta 181 (2018) 248–257.
[21] J. Ting, F. Mei, M.Y. Zhang, J.W. Qiu, Z. Hu, G. Yong, A novel cholesterol conjugated fluorescence probe for Cu2+ detection and bioimaging in living cells, Spectrochim. Acta 227 (2020), 117530.
[22] L. Wang, X.D. Yang, X.L. Chen, Y.P. Zhou, X.D. Lu, C.G. Yan, Y.K. Xu, R.Y. Liu, J.Q. Qu, A novel fluorescence probe based on triphenylamine Schiff base for bioimaging and responding to pH and Fe^{3+}, Mat Sci Eng C-Mater 72 (2017) 551–557.
[23] U. Bohm, S.W. Hell, R. Schmidt, 4Pi-RESOLFT nanoscopy, Nat. Commun. 7 (2016), 10504.
[24] M.T. Li, Z.L. Huang, Rethinking resolution estimation in fluorescence microscopy: from theoretical resolution criteria to super-resolution microscopy, Sci. China Life Sci. 63 (12) (2020) 1776–1785.
[25] X.X. Cui, Q. Fan, S.J. Shi, W.H. Wen, D.F. Chen, H.T. Guo, Y.T. Xu, F. Gao, R.Z. Nie, H.D. Ford, G.H. Tang, C.Q. Hou, B. Peng, A novel near-infrared nanomaterial with high quantum efficiency and its applications in real time in vivo imaging, Nanotechnology 29 (20) (2018), 205705.
[26] F. Ding, Y.B. Zhan, X.J. Lu, Y. Sun, Recent advances in near-infrared II fluorophores for multifunctional biomedical imaging, Chem. Sci. 9 (19) (2018) 4370–4380.
[27] R. Weissleder, A clearer vision for in vivo imaging, Nat. Biotechnol. 19 (4) (2001) 316–317.
[28] R. Weissleder, C.H. Tung, U. Mahmood, A. Bogdanov, In vivo imaging of tumors with protease-activated near-infrared fluorescent probes, Nat. Biotechnol. 17 (4) (1999) 375–378.
[29] K. Welsher, Z. Liu, S.P. Sherlock, J.T. Robinson, Z. Chen, D. Daranciang, H.J. Dai, A route to brightly fluorescent carbon nanotubes for near-infrared imaging in mice, Nat. Nanotechnol. 4 (11) (2009) 773–780.
[30] Y.L. Yang, F. Zhang, Molecular fluorophores for in vivo bioimaging in the second near-infrared window, Eur. J. Nucl. Med. Mol. Imag. 49 (9) (2022) 3226–3246.
[31] H.M. Gil, T.W. Price, K. Chelani, J.S.G. Bouillard, S.D.J. Calaminus, G.J. Stasiuk, NIR-quantum dots in biomedical imaging and their future, iScience 24 (3) (2021), 102189.
[32] J. Nicholas, H. Chen, K.R. Liu, I. Venu, D. Bolser, N.B. Saleh, J.H. Bisesi, W. Castleman, P.L. Ferguson, T. Sabo-Attwood, Utilization of near infrared fluorescence imaging to track and quantify the pulmonary retention of single-walled carbon nanotubes in mice, Nanoimpact 14 (2019), 100167.
[33] W.Q. Wang, X.W. He, M.Z. Du, C. Xie, W. Zhou, W. Huang, Q.L. Fan, Organic fluorophores for 1064 nm excited NIR-II fluorescence imaging, Front. Chem. 9 (2021), 769655.
[34] T. Repenko, A. Rix, S. Ludwanowski, D. Go, F. Kiessling, W. Lederle, A.J.C. Kuehne, Bio-degradable highly fluorescent conjugated polymer nanoparticles for bio-medical imaging applications, Nat. Commun. 8 (2017) 470.
[35] Z.H. Sheng, Y.X. Li, D.H. Hu, T.L. Min, D.Y. Gao, J.S. Ni, P.F. Zhang, Y.N. Wang, X. Liu, K. Li, H.R. Zheng, B.Z. Tang, Centimeter-deep NIR-II fluorescence imaging with nontoxic AIE probes in nonhuman primates, Research-China 2020 (2020), 4074593.
[36] A. Gnach, T. Lipinski, A. Bednarkiewicz, J. Rybka, J.A. Capobianco, Upconverting nanoparticles: assessing the toxicity, Chem. Soc. Rev. 44 (6) (2015) 1561–1584.
[37] J.K. Wang, Y.L. Zhu, C.A. Grimes, Q.Y. Cai, Multicolor lanthanide-doped CaS and SrS near-infrared stimulated luminescent nanoparticles with bright emission: application in broad-spectrum lighting, information coding, and bio-imaging, Nanoscale 11 (26) (2019) 12497–12501.
[38] G.T. Sun, Y. Xie, L.N. Sun, H.J. Zhang, Lanthanide upconversion and downshifting luminescence for biomolecules detection, Nanoscale Horiz 6 (10) (2021) 766–780.
[39] X.R. Song, S.H. Li, H.H. Guo, W.W. You, X.Y. Shang, R.F. Li, D.T. Tu, W. Zheng, Z. Chen, H.H. Yang, X.Y. Chen, Graphene-Oxide-modified lanthanide nanoprobes for tumor-targeted visible/NIR-II luminescence imaging, Angew. Chem., Int. Ed. 58 (52) (2019) 18981–18986.
[40] F. Wang, D. Banerjee, Y.S. Liu, X.Y. Chen, X.G. Liu, Upconversion nanoparticles in biological labeling, imaging, and therapy, Analyst 135 (8) (2010) 1839–1854.
[41] W. Tao, O.C. Farokhzad, Theranostic nanomedicine in the NIR-II window: classification, fabrication, and biomedical applications, Chem. Rev. 122 (6) (2022) 5405–5407.
[42] B.Z. Zheng, J.Y. Fan, B. Chen, X. Qin, J. Wang, F. Wang, R.R. Deng, X.G. Liu, Rare-earth doping in nanostructured inorganic materials, Chem. Rev. 122 (6) (2022) 5519–5603.

[43] M. Matulionyte, A. Skripka, A. Ramos-Guerra, A. Benayas, F. Vetrone, The coming of age of neodymium: redefining its role in rare earth doped nanoparticles, Chem. Rev. 123 (1) (2022) 515–554.

[44] X.Y. Zhu, X.H. Wang, H.X. Zhang, F. Zhang, Luminescence lifetime imaging based on lanthanide nanoparticles, Angew. Chem., Int. Ed. 61 (42) (2022), e202209378.

[45] D.K. Chatteriee, A.J. Rufalhah, Y. Zhang, Upconversion fluorescence imaging of cells and small animals using lanthanide doped nanocrystals, Biomaterials 29 (7) (2008) 937–943.

[46] F. Vetrone, R. Naccache, V. Mahalingam, C.G. Morgan, J.A. Capobianco, The active-core/active-shell approach: a strategy to enhance the upconversion luminescence in lanthanide-doped nanoparticles, Adv. Funct. Mater. 19 (18) (2009) 2924–2929.

[47] F. Vetrone, V. Mahalingam, J.A. Capobianco, Near-Infrared-to-Blue upconversion in colloidal $BaYF_5$:Tm^{3+}, Yb^{3+} nanocrystals, Chem. Mater. 21 (9) (2009) 1847–1851.

[48] J.H.S.K. Monteiro, Recent advances in luminescence imaging of biological systems using lanthanide(III) luminescent complexes, Molecules 25 (9) (2020) 2089.

[49] S. Ranjan, M.K.G. Jayakumar, Y. Zhang, Luminescent lanthanide nanomaterials: an emerging tool for theranostic applications, Nanomedicine-Uk 10 (9) (2015) 1477–1491.

[50] G.Q. Jin, Y.Y. Ning, J.X. Geng, Z.F. Jiang, Y. Wang, J.L. Zhang, Joining the journey to near infrared (NIR) imaging: the emerging role of lanthanides in the designing of molecular probes, Inorg. Chem. Front. 7 (2) (2020) 289–299.

[51] M. Zhang, Z.J. Wang, Y.L. Shao, Y.Y. Zhao, Z.H. Liu, Complement-opsonized NIR-IIb emissive immunotracers for dynamically monitoring neutrophils in inflammation-related diseases, Adv Mater 34 (34) (2022), 2203477.

[52] H. Li, X. Wang, D.X. Huang, G.Y. Chen, Recent advances of lanthanide-doped upconversion nanoparticles for biological applications, Nanotechnology 31 (7) (2020), 072001.

[53] C. Cao, Q.Y. Liu, M. Shi, W. Feng, F.Y. Li, Lanthanide-doped nanoparticles with upconversion and downshifting near-infrared luminescence for bioimaging, Inorg. Chem. 58 (14) (2019) 9351–9357.

[54] L. Prodi, E. Rampazzo, F. Rastrelli, A. Speghini, N. Zaccheroni, Imaging agents based on lanthanide doped nanoparticles, Chem. Soc. Rev. 44 (14) (2015) 4922–4952.

[55] X.Y. Zhu, X. Liu, H.X. Zhang, M.Y. Zhao, P. Pei, Y. Chen, Y.W. Yang, L.F. Lu, P. Yu, C.X. Sun, J. Ming, I.M. Abraham, A.M. El-Toni, A. Khan, F. Zhang, High-fidelity NIR-II multiplexed lifetime bioimaging with bright double interfaced lanthanide nanoparticles, Angew. Chem., Int. Ed. 60 (44) (2021) 23545–23551.

[56] J.J. Zhou, J.L. Leano, Z.Y. Liu, D.Y. Jin, K.L. Wong, R.S. Liu, J.C.G. Bunzli, Impact of lanthanide nanomaterials on photonic devices and smart applications, Small 14 (40) (2018), 1801882.

[57] H.H. Fu, Y.H. Ma, Y.S. Liu, M.C. Hong, Local-structure-dependent luminescence in lanthanide-doped inorganic nanocrystals for biological applications, Chem. Commun. 57 (24) (2021) 2970–2981.

[58] Y.Y. Ning, G.Q. Jin, M.X. Wang, S. Gao, J.L. Zhang, Recent progress in metal-based molecular probes for optical bioimaging and biosensing, Curr. Opin. Chem. Biol. 66 (2022), 102097.

[59] Z.C. Luo, D.H. Hu, D.Y. Gao, Z.G. Yi, H.R. Zheng, Z.H. Sheng, X.G. Liu, High-specificity in vivo tumor imaging using bioorthogonal NIR-IIb nanoparticles, Adv Mater 33 (49) (2021), 2102950.

[60] Z.M. Tao, X.N. Dang, X. Huang, M.D. Muzumdar, E.S. Xu, N.M. Bardhan, H.Q. Song, R.G. Qi, Y.J. Yu, T. Li, W. Wei, J. Wyckoff, M.J. Birrer, A.M. Belcher, P.P. Ghoroghchian, Early tumor detection afforded by in vivo imaging of near-infrared II fluorescence, Biomaterials 134 (2017) 202–215.

[61] Z.J. Li, Y.W. Zhang, H.E. La, R. Zhu, G. El-Banna, Y.Z. Wei, G. Han, Upconverting NIR photons for bioimaging, Nanomaterials-Basel 5 (4) (2015) 2148–2168.

[62] Y.X. Liu, L.Y. Li, Q.W. Guo, L. Wang, D.D. Liu, Z.W. Wei, J. Zhou, Novel Cs-based upconversion nanoparticles as dual-modal CT and UCL imaging agents for chemo-photothermal synergistic therapy, Theranostics 6 (10) (2016) 1491–1505.

[63] A. Xia, Y. Gao, J. Zhou, C.Y. Li, T.S. Yang, D.M. Wu, L.M. Wu, F.Y. Li, Core-shell $NaYF_4$:Yb^{3+},Tm^{3+}@Fe_xO_y nanocrystals for dual-modality T-2-enhanced magnetic resonance and NIR-to-NIR upconversion luminescent imaging of small-animal lymphatic node, Biomaterials 32 (29) (2011) 7200–7208.

[64] M. Liu, Z.Y. Shi, X. Wang, Y.T. Zhang, X.L. Mo, R.B. Jiang, Z.H. Liu, L. Fan, C.G. Ma, F. Shi, Simultaneous enhancement of red upconversion luminescence and CT contrast of NaGdF4:Yb,Er nanoparticles via Lu^{3+} doping, Nanoscale 10 (43) (2018) 20279–20288.

[65] F. Ren, H.H. Liu, H. Zhang, Z.L. Jiang, B. Xia, C. Genevois, T. He, M. Allix, Q. Sun, Z. Li, M.Y. Gao, Engineering NIR-IIb fluorescence of Er-based lanthanide nanoparticles for through-skull targeted imaging and imaging-guided surgery of orthotopic glioma, Nano Today 34 (2020), 100905.

[66] M.Y. Ahmad, H. Yue, T. Tegafaw, S.W. Liu, S.L. Ho, G.H. Lee, S.W. Nam, Y.M. Chang, Functionalized lanthanide oxide nanoparticles for tumor targeting, medical imaging, and therapy, Pharmaceutics 13 (11) (2021) 1890.

[67] B.P. Chhetri, A. Karmakar, A. Ghosh, Recent advancements in ln-ion-based upconverting nanomaterials and their biological applications, Part. Part. Syst. Char. 36 (8) (2019), 1900153.

[68] R.C. Lv, M. Feng, J. Liu, X. Jiang, H.J. Yuan, R.Y. Yan, J. Tian, Improved red emission and short-wavelength infrared luminescence under 808 nm laser for tumor theranostics, ACS Biomater. Sci. Eng. 5 (9) (2019) 4683–4691.

[69] Y. Chen, K.L. Ai, J.H. Liu, G.Y. Sun, Q. Yin, L.H. Lu, Multifunctional envelope-type mesoporous silica nanoparticles for pH-responsive drug delivery and magnetic resonance imaging, Biomaterials 60 (2015) 111–120.

[70] L.Y. Yao, Y. Hu, Z. Liu, X. Ding, J. Tian, J.X. Xiao, Luminescent lanthanide-collagen peptide framework for pH-controlled drug delivery, Mol. Pharm. 16 (2) (2019) 846–855.

[71] J.Y. Liao, L. Yang, S.T. Wu, Z.C. Yang, J.J. Zhou, D.Y. Jin, M. Guan, NIR-II emissive properties of 808 nm-excited lanthanide-doped nanoparticles for multiplexed in vivo imaging, J. Lumin. 242 (2022), 118597.

[72] G.C. Bao, S.H. Wen, G.G. Lin, J.L. Yuan, J. Lin, K.L. Wong, J.C.G. Bunzli, D.Y. Jin, Learning from lanthanide complexes: the development of dye-lanthanide nanoparticles and their biomedical applications, Coord. Chem. Rev. 429 (2021), 213642.

[73] X.X. Peng, X.F. Zhu, J.L. Zhang, Near Infrared (NIR) imaging: exploring biologically relevant chemical space for lanthanide complexes, J. Inorg. Biochem. 209 (2020), 111118.

[74] W.X. He, J. Yan, L.J. Wang, B. Lei, P. Hou, W.Y. Lu, P.X. Ma, A lanthanide-peptide-derived bacterium-like nanotheranostic with high tumor-targeting, -imaging and -killing properties, Biomaterials 206 (2019) 13–24.

[75] E. Ximendes, A. Benayas, D. Jaque, R. Marin, Quo vadis, nanoparticle-enabled in vivo fluorescence imaging? ACS Nano 15 (2) (2021) 1917–1941.

[76] K. Zhao, J. Sun, F. Wang, A. Song, K. Liu, H. Zhang, Lanthanide-based photothermal materials: fabrication and biomedical applications, ACS Appl. Bio Mater. 3 (7) (2020) 3975–3986.

[77] A.C. Croce, G. Bottiroli, Autofluorescence spectroscopy and imaging: a tool for biomedical research and diagnosis, Eur. J. Histochem. 58 (4) (2014) 320–337.

[78] L. Liang, N. Chen, Y.Y. Jia, Q.Q. Ma, J. Wang, Q. Yuan, W.H. Tan, Recent progress in engineering near-infrared persistent luminescence nanoprobes for time-resolved biosensing/bioimaging, Nano Res. 12 (6) (2019) 1279–1292.

[79] F. Lu, T. Zhao, X.J. Sun, Z.Q. Wang, Q.L. Fan, W. Huang, Rare-earth doped nanoparticles with narrow NIR-II emission for optical imaging with reduced autofluorescence, Chem. Res. Chin. Univ. 37 (4) (2021) 943–950.

[80] H.X. Zhang, Z.H. Chen, X. Liu, F. Zhang, A mini-review on recent progress of new sensitizers for luminescence of lanthanide doped nanomaterials, Nano Res. 13 (7) (2020) 1795–1809.

[81] S.H. Wen, J.J. Zhou, K.Z. Zheng, A. Bednarkiewicz, X.G. Liu, D.Y. Jin, Advances in highly doped upconversion nanoparticles, Nat. Commun. 9 (2018) 2415.

[82] R. Marin, D. Jaque, A. Benayas, Switching to the brighter lane: pathways to boost the absorption of lanthanide-doped nanoparticles, Nanoscale Horiz 6 (3) (2021) 209–230.

[83] J.W. Zhao, H.S. Hu, W.Q. Liu, X. Wang, Multifunctional NaYF4:Nd/NaDyF4 nanocrystals as a multimodal platform for NIR-II fluorescence and magnetic resonance imaging, Nanoscale Adv. 3 (2) (2021) 463–470.

[84] X. Wang, A. Yakovliev, T.Y. Ohulchanskyy, L. Wu, S.J. Zeng, X.J. Han, J.L. Qu, G.Y. Chen, Efficient erbium-sensitized core/shell nanocrystals for short wave infrared bioimaging, Adv. Opt. Mater. 6 (20) (2018), 1800690.

[85] M.Y. Zhao, R. Wang, B.H. Li, Y. Fan, Y.F. Wu, X.Y. Zhu, F. Zhang, Precise InVivo inflammation imaging using InSitu responsive cross-linking of glutathione-modified ultra-small NIR-II lanthanide nanoparticles, Angew. Chem., Int. Ed. 58 (7) (2019) 2050–2054.

[86] G.Y. Chen, T.Y. Ohulchanskyy, S. Liu, W.C. Law, F. Wu, M.T. Swihart, H. Agren, P.N. Prasad, Core/shell $NaGdF_4$:Nd^{3+}/$NaGdF_4$ nanocrystals with efficient near-infrared to near-infrared downconversion photoluminescence for bioimaging applications, ACS Nano 6 (4) (2012) 2969–2977.

[87] T. Wang, M. Yang, J.H. Huang, Y.Z. Zhao, H.L. Wang, S. Leng, J.X. Chen, G.Y. Sun, J.H. Liu, NIR-to-NIR UCL/T-1-weighted MR/CT multimodal imaging by $NaYbF_4$:Tm@$NaGdF_4$:Yb-PVP upconversion nanoparticles, Sci. Bull. 62 (13) (2017) 903–912.

[88] J.T. Xu, D. Yang, W. Han, S.M. Dong, T. Jia, F. He, H.T. Bi, S.L. Gai, L. Li, P.P. Yang, A novel strategy for markedly enhancing the red upconversion emission in Er3+/Tm3+ cooperated nanoparticles, J. Mater. Chem. C 6 (28) (2018) 7533–7540.

[89] Z.Y. Nie, X.X. Ke, D.N. Li, Y.L. Zhao, L.L. Zhu, R. Qiao, X.L. Zhang, $NaYF_4$:Yb,Er,Nd@$NaYF_4$:Nd upconversion nanocrystals capped with Mn:TiO_2 for 808 nm NIR-triggered photocatalytic applications, J. Phys. Chem. C 123 (37) (2019) 22959–22970.

[90] M. Wang, R. Mi, L. Wang, H.Q. Chen, Preparation of cyanine dye sensitized upconversion luminescent nanoprobe and hypochlorous acid detection by light-emitting energy transfer, J. Lumin. 239 (2021), 118395.

[91] Z.Q. Liang, Z.Y. Zou, X. Yan, X.B. Zhang, D.D. Song, C.Q. Ye, X.M. Wang, X.T. Tao, Conjugate and non-conjugate controls of a sensitizer to enhance dye-sensitized upconversion luminescence, J. Mater. Chem. C 10 (6) (2022) 2205–2212.

[92] W. Shao, G.Y. Chen, A. Kuzmin, H.L. Kutscher, A. Pliss, T.Y. Ohulchanskyy, P.N. Prasad, Tunable narrow band emissions from dye-sensitized core/shell/shell nanocrystals in the second near-infrared biological window, J. Am. Chem. Soc. 138 (50) (2016) 16192–16195.

[93] Q.Y. Liu, X.M. Zou, Y.B. Shi, B. Shen, C. Cao, S.M. Cheng, W. Feng, F.Y. Li, An efficient dye-sensitized NIR emissive lanthanide nanomaterial and its application in fluorescence-guided peritumoral lymph node dissection, Nanoscale 10 (26) (2018) 12573–12581.

[94] Z. Liu, B. Yun, Y. Han, Z. Jiang, H. Zhu, F. Ren, Z. Li, Dye-sensitized rare earth nanoparticles with up/down conversion luminescence for on-demand gas therapy of glioblastoma guided by NIR-II fluorescence imaging, Adv Healthc Mater 11 (3) (2022), e2102042.

[95] Q. Wang, T. Liang, J. Wu, Z. Li, Z. Liu, Dye-sensitized rare earth-doped nanoparticles with boosted NIR-IIb emission for dynamic imaging of vascular network-related disorders, ACS Appl. Mater. Interfaces 13 (25) (2021) 29303–29312.

[96] R.C. Lv, F. Yang, X. Jiang, B. Hu, X.H. Zhang, X.L. Chen, J. Tian, Plasmonic modulated upconversion fluorescence by adjustable distributed gold nanoparticles, J. Lumin. 220 (2020), 116974.

[97] Y.S. Zhu, W. Xu, G.Q. Li, S.B. Cui, X.Y. Liu, H.W. Song, Plasmonic enhancement of the upconversion fluorescence in YVO4:Yb^{3+}, Er^{3+} nanocrystals based on the porous Ag film, Nanotechnology 26 (14) (2015), 145602.

[98] Y.H. Ma, L.P. Zhang, L. Wang, L. Wang, H.Q. Chen, Preparation of gold nanoparticle coated $NaYF_4$:Yb,Er,Gd nanoparticles and their application for AFP detection in the red region, Anal Methods-Uk 9 (20) (2017) 2977–2982.

[99] Y. Fan, L. Liu, F. Zhang, Exploiting lanthanide-doped upconversion nanoparticles with core/shell structures, Nano Today 25 (2019) 68–84.

[100] H.X. Zhang, Y. Fan, P. Pei, C.X. Sun, L.F. Lu, F. Zhang, Tm^{3+}-Sensitized NIR-II fluorescent nanocrystals for in vivo information storage and decoding, Angew. Chem., Int. Ed. 58 (30) (2019) 10153–10157.

[101] S.H. Yu, J. Xu, X.Y. Shang, W. Zheng, P. Huang, R.F. Li, D.T. Tu, X.Y. Chen, A dual-excitation decoding strategy based on NIR hybrid nanocomposites for high-accuracy thermal sensing, Adv. Sci. 7 (20) (2020), 2001589.

[102] W. Gao, Z.Y. Sun, Q.Y. Han, S.S. Han, X.T. Cheng, Y.K. Wang, X.W. Yan, J. Dong, Enhancing upconversion emission of Er^{3+} in single beta-NaYF4 microrod through constructing different inert and active shells with doping Yb^{3+} ions, J. Alloys Compd. 857 (2021), 157578.

[103] M. Sengar, A.K. Narula, Lanthanide doped luminescent $NaGdF_4$:Nd^{3+},Yb^{3+}@CaF_2:Eu^{3+} nanoparticles for dual-mode (visible and NIR) luminescence, J. Solid State Chem. 295 (2021), 121913.

[104] Y.B. Li, M.Y. Jiang, Z.L. Xue, S.J. Zeng, 808 nm light triggered lanthanide nanoprobes with enhanced down-shifting emission beyond 1500 nm for imaging-guided resection surgery of tumor and vascular visualization, Theranostics 10 (15) (2020) 6875–6885.

[105] B.Y. Ren, B. Chen, J.X. Zhao, Y. Guo, X. Zhang, X. Chen, Y.Y. Du, Z.Q. Deng, G.Y. Zhu, F. Wang, Synthesis of core-shell ScF3 nanoparticles for thermal enhancement of upconversion, Chem. Mater. 33 (1) (2021) 158–163.

[106] J.X. Cao, L. Zhang, X. Ding, D. Liu, B. Su, J.Y. Shi, Dual-targeting peptides RGD10-NGR9-conjugated lanthanide Nanoparticle@Polydopamine as upconversion nanoprobes for in vivo imaging of lung cancer, Small Methods 4 (12) (2020), 2000648.

[107] C. Cao, G.S. Li, Y. Xie, C. Hong, Y. Li, Er^{3+} doped core-shell nanoparticles with large enhanced near-infrared luminescence for in vivo imaging, Inorg. Chem. Commun. 126 (2021), 108468.

[108] W. Wang, Z. Feng, B. Li, Y.L. Chang, X. Li, X. Yan, R.Z. Chen, X.M. Yu, H.Y. Zhao, G.Y. Lu, X.G. Kong, J. Qian, X.M. Liu, Er^{3+} self-sensitized nanoprobes with enhanced 1525 nm downshifting emission for NIR-IIb in vivo bio-imaging, J. Mater. Chem. B 9 (12) (2021) 2899–2908.

[109] R. Wang, X.M. Li, L. Zhou, F. Zhang, Epitaxial seeded growth of rare-earth nanocrystals with efficient 800 nm near-infrared to 1525 nm short-wavelength infrared downconversion photoluminescence for in vivo bioimaging, Angew. Chem., Int. Ed. 53 (45) (2014) 12086–12090.

[110] Y.T. Zhong, Z.R. Ma, S.J. Zhu, J.Y. Yue, M.X. Zhang, A.L. Antaris, J. Yuan, R. Cui, H. Wan, Y. Zhou, W.Z. Wang, N.F. Huang, J. Luo, Z.Y. Hu, H.J. Dai, Boosting the down-shifting luminescence of rare-earth nanocrystals for biological imaging beyond 1500 nm, Nat. Commun. 8 (2017) 737.

[111] C.L. Wang, H.X. Lin, X.G. Ge, J. Mu, L.C. Su, X. Zhang, M. Niu, H.H. Yang, J.B. Song, Dye-sensitized downconversion nanoprobes with emission beyond 1500 nm for ratiometric visualization of cancer redox state, Adv. Funct. Mater. 31 (16) (2021), 2009942.

[112] B. Xue, D. Wang, L.P. Tu, D.P. Sun, P.T. Jing, Y.L. Chang, Y.L. Zhang, X.M. Liu, J. Zuo, J. Song, J.L. Qu, E.J. Meijer, H. Zhang, X.G. Kong, Ultrastrong absorption meets ultraweak absorption: unraveling the energy-dissipative routes for dye-sensitized upconversion luminescence, J. Phys. Chem. Lett. 9 (16) (2018) 4625.

[113] X.D. Wang, R.R. Valiev, T.Y. Ohulchanskyy, H. Agren, C.H. Yang, G.Y. Chen, Dye-sensitized lanthanide-doped upconversion nanoparticles, Chem. Soc. Rev. 46 (14) (2017) 4150–4167.

[114] J. Liu, P. Geiregat, L. Pilia, R. Van Deun, F. Artizzu, Molecular size matters: ultrafast dye singlet sensitization pathways to bright nanoparticle emission, Adv. Opt. Mater. 9 (7) (2021), 2001678.

[115] B.Z. Zheng, D.N. Zhong, T.T. Xie, J. Zhou, W.L. Li, A. Ilyas, Y.H. Lu, M. Zhou, R.R. Deng, Near-infrared photosensitization via direct triplet energy transfer from lanthanide nanoparticles, Chem-Us 7 (6) (2021) 1615–1625.

[116] X.Y. Zhao, M.F. Wang, Z.W. Cai, D.Y. Xia, L. Zhao, Q.W. Song, Y.R. Qin, W. Wei, Optimizing the performance of dye-sensitized upconversion nanoparticles, Dyes Pigments 192 (2021), 109428.

[117] T. Liang, Q.R. Wang, Z. Li, P.P. Wang, J.J. Wu, M.M. Zuo, Z.H. Liu, Removing the obstacle of dye-sensitized upconversion luminescence in aqueous phase to achieve high-contrast deep imaging in vivo, Adv. Funct. Mater. 30 (16) (2020), 1910765.

[118] Z.Z. Yu, C.K. Lim, W.K. Chan, Y. Chen, W. Shao, Y. Zhang, P.N. Prasad, T.T.Y. Tan, Dye-sensitized lanthanide-doped upconversion nanoparticles for water detection in organic solvents, ACS Appl. Nano Mater. 4 (12) (2021) 14069–14076.

[119] D. Wang, D.P. Wang, A. Kuzmin, A. Pliss, W. Shao, J. Xia, J.L. Qu, P.N. Prasad, ICG-sensitized NaYF4:Er nanostructure for theranostics, Adv. Opt. Mater. 6 (12) (2018), 1701142.

[120] J. Liu, H. He, D. Xiao, S. Yin, W. Ji, S. Jiang, D. Luo, B. Wang, Y. Liu, Recent advances of plasmonic nanoparticles and their applications, Materials 11 (10) (2018) 1833.

[121] B. Shao, Z.W. Yang, J. Li, J.Z. Yang, Y.D. Wang, J.B. Qiu, Z.G. Song, Au nanoparticles embedded inverse opal photonic crystals as substrates for upconversion emission enhancement, J. Am. Ceram. Soc. 100 (3) (2017) 988–997.

[122] K.A. Willets, R.P. Van Duyne, Localized surface plasmon resonance spectroscopy and sensing, Annu. Rev. Phys. Chem. 58 (2007) 267–297.

[123] K.H. Drexhage, Influence of a dielectric interface on fluorescence decay time, Bull. Am. Phys. Soc. 14 (8) (1969) 873–&.

[124] I. Gryczynski, J. Malicka, E. Holder, N. DiCesare, J.R. Lakowicz, Effects of metallic silver particles on the emission properties of [Ru(bpy)(3)](2+), Chem. Phys. Lett. 372 (3–4) (2003) 409–414.

[125] S.K. Maurya, S.P. Tiwari, A. Kumar, K. Kumar, Plasmonic enhancement of upconversion emission in Ag@$NaYE_4$:Er^{3+}/Yb^{3+} phosphor, J. Rare Earths 36 (9) (2018) 903–910.

[126] K.Y. Zhang, F. Lu, Z. Cai, S.T. Song, L.P. Jiang, Q.H. Min, X.C. Wu, J.J. Zhu, Plasmonic modulation of the upconversion luminescence based on gold nanorods for designing a new strategy of sensing MicroRNAs, Anal. Chem. 92 (17) (2020) 11795–11801.

[127] Y. Zheng, Y. Wang, Y.B. Guo, L. Chen, Plasmon-tuned upconversion luminescence in silanized NaYF4:Yb,Er nanocrystals via ultra-thin gold film, Mater. Res. Bull. 113 (2019) 209–214.

[128] L.X. Wang, S.L. Guo, D.M. Liu, J.J. He, J. Zhou, K. Zhang, Y. Wei, Y. Pan, C. Gao, Z. Yuan, D.Y. Lei, X.J. Xie, L. Huang, Plasmon-enhanced blue upconversion luminescence by indium nanocrystals, Adv. Funct. Mater. 29 (29) (2019), 1901142.

[129] A.K. Soni, R. Joshi, B.P. Singh, N.N. Kumar, R.S. Ningthoujam, Near-infrared- and magnetic-field-responsive $NaYF_4$:Er^{3+}/Yb^{3+} @SiO_2@AuNP@Fe_3O_4 nanocomposites for hyperthermia applications induced by fluorescence resonance energy transfer and surface plasmon absorption, ACS Appl. Nano Mater. 2 (11) (2019) 7350–7361.

[130] B. Lin, J. Liu, Y.X. Wang, F. Yang, L.Y. Huang, R.C. Lv, Enhanced upconversion luminescence-guided synergistic antitumor therapy based on photodynamic therapy and immune checkpoint blockade, Chem. Mater. 32 (11) (2020) 4627–4640.

[131] X. Chen, D.L. Zhou, W. Xu, J.Y. Zhu, G.C. Pan, Z. Yin, H. Wang, Y.S. Zhu, S.B. Cui, H.W. Song, Fabrication of Au-Ag nanocage@NaYF4@NaYF4: Yb,Er core-shell hybrid and its tunable upconversion enhancement, Sci Rep-Uk 7 (2017), 41079.

[132] R.K. Sharma, A.V. Mudring, P. Ghosh, Recent trends in binary and ternary rare-earth fluoride nanophosphors: how structural and physical properties influence optical behavior, J. Lumin. 189 (2017) 44–63.

[133] J. Li, W.N. Zhang, C.H. Lu, Z.Z. Lou, B.J. Li, Nonmetallic plasmon induced 500-fold enhancement in the upconversion emission of the UCNPs/WO3-x hybrid, Nanoscale Horiz 4 (4) (2019) 999–1005.

[134] Y.T. Zhong, Z.R. Ma, F.F. Wang, X. Wang, Y.J. Yang, Y.L. Liu, X. Zhao, J.C. Li, H.T. Du, M.X. Zhang, Q.H. Cui, S.J. Zhu, Q.C. Sun, H. Wan, Y. Tian, Q. Liu, W.Z. Wang, K.C. Garcia, H.J. Dai, In vivo molecular imaging for immunotherapy using ultra-bright near-infrared-IIb rare-earth nanoparticles, Nat. Biotechnol. 37 (11) (2019) 1322.

[135] J. Zhu, L.F. Lu, Y. Fan, C.C. Zhou, A novel lanthanide-based NIR-II nanoprobe for lung squamous cell carcinoma identification, Biomater Sci-Uk 9 (19) (2021) 6568–6573.

[136] J. Yao, G. López-Peña, J. Lifante, M.C. Iglesias-de la Cruz, R. Marin, E. Martín Rodríguez, D. Jaque, D.H. Ortgies, (INVITED)Adjustable near-infrared fluorescence lifetime emission of biocompatible rare-earth-doped nanoparticles for in vivo multiplexing, Opt. Mater. X 17 (2023), 100225.

[137] X.L. Li, M.Y. Jiang, S.J. Zeng, H.R. Liu, Polydopamine coated multifunctional lanthanide theranostic agent for vascular malformation and tumor vessel imaging beyond 1500 nm and imaging-guided photothermal therapy, Theranostics 9 (13) (2019) 3866–3878.

[138] X.L. Li, M.Y. Jiang, Y.B. Li, Z.L. Xue, S.J. Zeng, H.R. Liu, 808 nm laser-triggered NIR-II emissive rare-earth nanoprobes for small tumor detection and blood vessel imaging, Materials Science and Engineering C-Materials for Biological Applications 100 (2019) 260–268.

[139] P.Y. Wang, Y. Fan, L.F. Lu, L. Liu, L.L. Fan, M.Y. Zhao, Y. Xie, C.J. Xu, F. Zhang, NIR-II nanoprobes in-vivo assembly to improve image-guided surgery for metastatic ovarian cancer, Nat. Commun. 9 (2018) 2898.

[140] F. Ren, L.H. Ding, H.H. Liu, Q. Huang, H. Zhang, L.J. Zhang, J.F. Zeng, Q. Sun, Z. Li, M.Y. Gao, Ultra-small nanocluster mediated synthesis of Nd^{3+}-doped core-shell nanocrystals with emission in the second near-infrared window for multimodal imaging of tumor vasculature, Biomaterials 175 (2018) 30–43.

[141] H. Li, X. Wang, X.L. Li, S.J. Zeng, G.Y. Chen, Clearable shortwave-infrared-emitting NaErF4 nanoparticles for noninvasive dynamic vascular imaging, Chem. Mater. 32 (8) (2020) 3365–3375.

[142] M. Zhang, W. Zheng, Y. Liu, P. Huang, Z. Gong, J. Wei, Y. Gao, S. Zhou, X. Li, X. Chen, A new class of blue-LED-excitable NIR-II luminescent nanoprobes based on lanthanide-doped CaS nanoparticles, Angew Chem. Int. Ed. Engl. 58 (28) (2019) 9556–9560.

[143] Y.B. Li, S.J. Zeng, J.H. Hao, Non-invasive optical guided tumor metastasis/vessel imaging by using lanthanide nanoprobe with enhanced down-shifting emission beyond 1500 nm, ACS Nano 13 (1) (2019) 248–259.

[144] Z. Chen, W. Zheng, P. Huang, D.T. Tu, S.Y. Zhou, M.D. Huang, X.Y. Chen, Lanthanide-doped luminescent nano-bioprobes for the detection of tumor markers, Nanoscale 7 (10) (2015) 4274–4290.

[145] Y.B. Li, X.L. Li, Z.L. Xue, M.Y. Jiang, S.J. Zeng, J.H. Hao, Second near-infrared emissive lanthanide complex for fast renal-clearable in vivo optical bioimaging and tiny tumor detection, Biomaterials 169 (2018) 35–44.

[146] M.Y. Zhao, B.H. Li, Y.F. Wu, H.S. He, X.Y. Zhu, H.X. Zhang, C.R. Dou, L.S. Feng, Y. Fan, F. Zhang, A tumor-microenvironment-responsive lanthanide-cyanine FRET sensor for NIR-II luminescence-lifetime in situ imaging of hepatocellular carcinoma, Adv Mater 32 (28) (2020), 2001172.

[147] Z.J. Wang, M. Zhang, S.Y. Chi, M.T. Zhu, C.X. Wang, Z.H. Liu, Brain tumor cell membrane-coated lanthanide-doped nanoparticles for NIR-IIb luminescence imaging and surgical navigation of glioma, Advanced Healthcare Materials 11 (16) (2022), 2200521.
[148] A. Nexha, J.J. Carvajal, M.C. Pujol, F. Diaz, M. Aguilo, Lanthanide doped luminescence nanothermometers in the biological windows: strategies and applications, Nanoscale 13 (17) (2021) 7913–7987.
[149] R. Pinol, J. Zeler, C.D.S. Brites, Y.Y. Gu, P. Tellez, A.N.C. Neto, T.E. da Silva, R. Moreno-Loshuertos, P. Fernandez-Silva, A.I. Gallego, L. Martinez-Lostao, A. Martinez, L.D. Carlos, A. Millan, Real-time intracellular temperature imaging using lanthanide bearing polymeric micelles, Nano Lett. 20 (9) (2020) 6466–6472.
[150] X.J. Zhu, W. Feng, J. Chang, Y.W. Tan, J.C. Li, M. Chen, Y. Sun, F.Y. Li, Temperature-feedback upconversion nanocomposite for accurate photothermal therapy at facile temperature, Nat. Commun. 7 (2016), 10437.
[151] N. Kong, Q. Hu, Y.K. Wu, X.J. Zhu, Lanthanide luminescent nanocomposite for non-invasive temperature monitoring in vivo, Chem. Eur J. 28 (17) (2022), e202104237.
[152] C.D.S. Brites, S. Balabhadra, L.D. Carlos, Lanthanide-based thermometers: at the cutting-edge of luminescence thermometry, Adv. Opt. Mater. 7 (5) (2019), 1801239.
[153] J.L. Wang, X.Y. Hu, C.G. Han, S.Y. Hou, H.S. Wang, F. Zheng, Lanthanide complexes for tumor diagnosis and therapy by targeting sialic acid, ACS Nano (2022) 14827–14837.
[154] F. Yang, A. Skripka, A. Benayas, X.K. Dong, S.H. Hong, F.Q. Ren, J.K. Oh, X.Y. Liu, F. Vetrone, D.L. Ma, An integrated multifunctional nanoplatform for deep-tissue dual-mode imaging, Adv. Funct. Mater. 28 (11) (2018), 1706235.
[155] J.T. Xu, A. Gulzar, P.P. Yang, H.T. Bi, D. Yang, S.L. Gai, F. He, J. Lin, B.G. Xing, D.Y. Jin, Recent advances in near-infrared emitting lanthanide-doped nanoconstructs: mechanism, design and application for bioimaging, Coord. Chem. Rev. 381 (2019) 104–134.
[156] J.Y. Park, Y. Chang, G.H. Lee, Multi-Modal imaging and cancer therapy using lanthanide oxide nanoparticles: current status and perspectives, Curr. Med. Chem. 22 (5) (2015) 569–581.
[157] Y. Dai, D.P. Yang, D.P. Yu, C. Cao, Q.H. Wang, S.H. Xie, L. Shen, W. Feng, F.Y. Li, Mussel-inspired polydopamine-coated lanthanide nanoparticles for NIR-II/CT dual imaging and photothermal therapy, Acs Appl Mater Inter 9 (32) (2017) 26674–26683.
[158] S. Lu, D. Tu, P. Hu, J. Xu, R. Li, M. Wang, Z. Chen, M. Huang, X. Chen, Multifunctional nano-bioprobes based on rattle-structured upconverting luminescent nanoparticles, Angew Chem. Int. Ed. Engl. 54 (27) (2015) 7915–7919.
[159] F.Y. Xu, Y.M. Zhao, M. Hu, P. Zhang, N. Kong, R.Y. Liu, C.C. Liu, S.K. Choi, Lanthanide-doped core-shell nanoparticles as a multimodality platform for imaging and photodynamic therapy, Chem. Commun. 54 (68) (2018) 9525–9528.
[160] D. Gonzalez-Mancebo, A.I. Becerro, T.C. Rojas, A. Olivencia, A. Corral, M. Balcerzyk, E. Cantelar, F. Cusso, M. Ocana, Room temperature synthesis of water-dispersible $Ln(^{3+})$:CeF_3 (Ln = Nd, Tb) nanoparticles with different morphology as bimodal probes for fluorescence and CT imaging, J. Colloid Interface Sci. 520 (2018) 134–144.
[161] R. An, P.P. Lei, P. Zhang, X. Xu, J. Feng, H.J. Zhang, Near-infrared optical and X-ray computed tomography dual-modal imaging probe based on novel lanthanide-doped K0.3Bi0.7F2.4 upconversion nanoparticles, Nanoscale 10 (3) (2018) 1394–1402.
[162] A.E. D'Achille, R. Gonzalez-Rodriguez, E. Campbell, B.H. Lee, J.L. Coffer, A.V. Naumov, Rare-earth-doped cerium oxide nanocubes for biomedical near-infrared and magnetic resonance imaging, ACS Biomater. Sci. Eng. 6 (12) (2020) 6971–6980.
[163] A.C. Harnden, D. Parker, N.J. Rogers, Employing paramagnetic shift for responsive MRI probes, Coord. Chem. Rev. 383 (2019) 30–42.
[164] S.L. Mekuria, K.D. Addisu, H.Y. Chou, B.Z. Hailemeskel, H.C. Tsai, Potential fluorescence and magnetic resonance imaging modality using mixed lanthanide oxide nanoparticles, Colloids Surf., B 167 (2018) 54–62.
[165] Y.M. Feng, Q.B. Xiao, Y.H. Zhang, F.J. Li, Y.F. Li, C.Y. Li, Q.B. Wang, L.Y. Shi, H.Z. Lin, Neodymium-doped NaHoF4 nanoparticles as near-infrared luminescent/T-2-weighted MR dual-modal imaging agents in vivo, J. Mater. Chem. B 5 (3) (2017) 504–510.
[166] Z.J. Wang, T.T. Zhang, L. Pi, H.J. Xiang, P.L. Dong, C.C. Lu, T. Jin, Large-scale one-pot synthesis of water-soluble and biocompatible upconversion nanoparticles for dual-modal imaging, Colloids Surf., B 198 (2021), 111480.
[167] G.N. Zhu, L.P. Chen, F.X. Zeng, L. Gu, X.F. Yu, X. Li, J. Jiang, G. Guo, J.Y. Cao, K. Tang, H.Y. Zhu, H.E. Daldrup-Link, M. Wu, $GdVO_4$:Eu^{3+},Bi^{3+} nanoparticles as a contrast agent for MRI and luminescence bioimaging, ACS Omega 4 (14) (2019) 15806–15814.
[168] S. He, N.J.J. Johnson, V.A.N. Huu, E. Cory, Y.R. Huang, R.L. Sah, J.V. Jokerst, A. Almutairi, Simultaneous enhancement of photoluminescence, MRI relaxivity, and CT contrast by tuning the interfacial layer of lanthanide heteroepitaxial nanoparticles, Nano Lett. 17 (8) (2017) 4873–4880.
[169] C. Herlan, S. Brase, Lanthanide conjugates as versatile instruments for therapy and diagnostics, Dalton Trans. 49 (8) (2020) 2397–2402.
[170] Y.Y. Ning, S. Chen, H. Chen, J.X. Wang, S.Q. He, Y.W. Liu, Z. Cheng, J.L. Zhang, A proof-of-concept application of water-soluble ytterbium(III) molecular probes in in vivo NIR-II whole body bioimaging, Inorg. Chem. Front. 6 (8) (2019) 1962–1967.
[171] P.F. Peng, N. Wu, L.X. Ye, F.L. Jiang, W. Feng, F.Y. Li, Y.S. Liu, M.C. Hong, Biodegradable inorganic upconversion nanocrystals for in vivo applications, ACS Nano 14 (12) (2020) 16672–16680.
[172] Y. Huang, A. Skripka, L. Labrador-Paez, F. Sanz-Rodriguez, P. Haro-Gonzalez, D. Jaque, F. Rosei, F. Vetrone, Upconverting nanocomposites with combined photothermal and photodynamic effects, Nanoscale 10 (2) (2018) 791–799.
[173] J. Yan, B. Li, P.P. Yang, J. Lin, Y.L. Dai, Progress in light-responsive lanthanide nanoparticles toward deep tumor theranostics, Adv. Funct. Mater. 31 (42) (2021), 2104325.
[174] X.Z. Ai, M. Hu, Z.M. Wang, L.N. Lyu, W.M. Zhang, J. Li, H.H. Yang, J. Lin, B.G. Xing, Enhanced cellular ablation by attenuating hypoxia status and reprogramming tumor-associated macrophages via NIR light-responsive upconversion nanocrystals, Bioconjugate Chem. 29 (4) (2018) 928–938.
[175] M. Zou, Y.J. Zhao, B.B. Ding, F. Jiang, Y.Q. Chen, P.A. Ma, J. Lin, NIR-triggered biodegradable MOF-coated upconversion nanoparticles for synergetic chemodynamic/photodynamic therapy with enhanced efficacy, Inorg. Chem. Front. 8 (10) (2021) 2624–2633.
[176] Y. Li, J.L. Tang, D.X. Pan, L.D. Sun, C.Y. Chen, Y. Liu, Y.F. Wang, S. Shi, C.H. Yan, A versatile imaging and therapeutic platform based on dual-band luminescent lanthanide nanoparticles toward tumor metastasis inhibition, ACS Nano 10 (2) (2016) 2766–2773.
[177] M. Wang, Z. Chen, W. Zheng, H.M. Zhu, S. Lu, E. Ma, D.T. Tu, S.Y. Zhou, M.D. Huang, X.Y. Chen, Lanthanide-doped upconversion nanoparticles electrostatically coupled with photosensitizers for near-infrared-triggered photodynamic therapy, Nanoscale 6 (14) (2014) 8274–8282.
[178] J. Liu, L. Huang, X.M. Tian, X.M. Chen, Y.Z. Shao, F.K. Xie, D.H. Chen, L. Li, Magnetic and fluorescent Gd_2O_3:Yb^{3+}/Ln(3+) nanoparticles for simultaneous upconversion luminescence/MR dual modal imaging and NIR-induced photodynamic therapy, Int. J. Nanomed. 12 (2017) 1–14.
[179] F. Yang, J. Liu, X. Jiang, W.W. Wu, Z.N. Wang, Q. Zeng, R.C. Lv, Mesoporous semiconductors combined with upconversion nanoparticles for enhanced photodynamic therapy under near infrared light, RSC Adv. 9 (30) (2019) 17273–17280.
[180] S. Wang, Z. Wei, L. Li, X.H. Ning, Y.X. Liu, Luminescence imaging-guided triple-collaboratively enhanced photodynamic therapy by bioresponsive lanthanide-based nanomedicine, Nanomed-Nanotechnol 29 (2020), 102265.
[181] Y.Y. Liu, X.F. Meng, W.B. Bu, Upconversion-based photodynamic cancer therapy, Coord. Chem. Rev. 379 (2019) 82–98.
[182] L. Zhao, X.Q. Ge, G.H. Yan, X. Wang, P.F. Hu, L.Y. Shi, O.S. Wolfbeis, H.J. Zhang, L.N. Sun, Double-mesoporous core-shell nanosystems based on platinum nanoparticles functionalized with lanthanide complexes for in vivo magnetic resonance imaging and photothermal therapy, Nanoscale 9 (41) (2017) 16012–16023.
[183] H.R. Chen, F.X. Wu, X.Y. Xie, W. Wang, Q.Q. Li, L.P. Tu, B. Li, X.G. Kong, Y.L. Chang, Hybrid nanoplatform: enabling a precise antitumor strategy via dual-modal imaging-guided photodynamic/chemo-/immunosynergistic therapy, ACS Nano 15 (12) (2021) 20643–20655.
[184] T. Zhou, Q.Y. Cheng, L. Zhang, D.T. Zhang, L. Li, T.Y. Jiang, L. Huang, H. Xu, M. Hu, S. Jing, Ferrocene-functionalized core-shell lanthanide-doped upconversion nanoparticles: NIR light promoted chemodynamic therapy and luminescence imaging of solid tumors, Chem Eng J 438 (2022), 135637.
[185] Q.X. Wang, Y.F. Yang, X.F. Yang, Y. Pan, L.D. Sun, W.Y. Zhang, Y.L. Shao, J. Shen, J. Lin, L.L. Li, C.H. Yan, Upconverted/downshifted NaLnF4 and metal-organic framework heterostructures boosting NIR-II imaging-guided photodynamic immunotherapy toward tumors, Nano Today 43 (2022), 101439.
[186] M.Y. Jiang, H.R. Liu, S.J. Zeng, J.H. Hao, A general in situ growth strategy of designing theranostic NaLnF(4)@Cu2-xS nanoplatform for in vivo NIR-II optical imaging beyond 1500 nm and photothermal therapy, Adv Ther-Germany 2 (6) (2019), 1800153.
[187] Y. Li, C. Chen, F.F. Liu, J.L. Liu, Engineered lanthanide-doped upconversion nanoparticles for biosensing and bioimaging application, Microchim. Acta 189 (3) (2022) 109.
[188] Y.X. Liu, X.J. Zhu, Z. Wei, W. Feng, L.Y. Li, L.Y. Ma, F.Y. Li, J. Zhou, Customized photothermal therapy of subcutaneous orthotopic cancer by multichannel luminescent nanocomposites, Adv Mater 33 (30) (2021), 2008615.
[189] X.K. Sun, J. Sun, B. Dong, G.S. Huang, L. Zhang, W.H. Zhou, J.K. Lv, X.R. Zhang, M. Liu, L. Xu, X. Bai, W. Xu, Y.D. Yang, X.L. Song, H.W. Song, Noninvasive temperature monitoring for dual-modal tumor therapy based on lanthanide-doped up-conversion nanocomposites, Biomaterials 201 (2019) 42–52.
[190] X. Ding, J.H. Liu, D.P. Liu, J.Q. Li, F. Wang, L.J. Li, Y.H. Wang, S.Y. Song, H.J. Zhang, Multifunctional core/satellite polydopamine@Nd^{3+}-sensitized upconversion nanocomposite: a single 808 nm near-infrared light-triggered theranostic platform for in vivo imaging-guided photothermal therapy, Nano Res. 10 (10) (2017) 3434–3446.
[191] X. Wang, H. Li, F. Li, X.J. Han, G.Y. Chen, Prussian blue-coated lanthanide-doped core/shell/shell nanocrystals for NIR-II image-guided photothermal therapy, Nanoscale 11 (45) (2019) 22079–22088.
[192] B. Liu, J. Sun, J.J. Zhu, B. Li, C. Ma, X.Q. Gu, K. Liu, H.J. Zhang, F. Wang, J.J. Su, Y. Yang, Injectable and NIR-responsive DNA-inorganic hybrid hydrogels with outstanding photothermal therapy, Adv Mater 32 (39) (2020), 2004460.
[193] A. Skripka, V. Karabanovas, G. Jarockyte, R. Marin, V. Tam, M. Cerruti, R. Rotomskis, F. Vetrone, Decoupling theranostics with rare earth doped nanoparticles, Adv. Funct. Mater. 29 (12) (2019).
[194] J. Zuo, L.P. Tu, Q.Q. Li, Y.S. Feng, I. Que, Y.L. Zhang, X.M. Liu, B. Xue, L.J. Cruz, Y.L. Chang, H. Zhang, X.G. Kong, Near infrared light sensitive ultraviolet-blue nanophotoswitch for imaging-guided "Off-On" therapy, ACS Nano 12 (4) (2018) 3217–3225.
[195] Z. Liu, B.F. Yun, Y.B. Han, Z.L. Jiang, H.Q. Zhu, F. Ren, Z. Li, Dye-sensitized rare earth nanoparticles with up/down conversion luminescence for on-demand gas

therapy of glioblastoma guided by NIR-II fluorescence imaging, Advanced Healthcare Materials 11 (3) (2022), 2102042.
[196] J. Wang, N. Huang, Q. Peng, X.Y. Cheng, W.K. Li, Temperature/pH dual-responsive and luminescent drug carrier based on PNIPAM-MAA/lanthanide-polyoxometalates for controlled drug delivery and imaging in HeLa cells, Mater. Chem. Phys. 239 (2020), 121994.
[197] J.Y.R. Silva, Y.G. Proenza, L.L. da Luz, S.D. Araujo, M.A. Gomes, S. Alves, T.A. Soares, R.L. Longo, A thermo-responsive adsorbent-heater-thermometer nanomaterial for controlled drug release: (ZIF-8,EuxTby)@AuNP core-shell, Materials Science and Engineering C-Materials for Biological Applications 102 (2019) 578–588.
[198] S. Lu, D.T. Tu, P. Hu, J. Xu, R.F. Li, M. Wang, Z. Chen, M.D. Huang, X.Y. Chen, Multifunctional nano-bioprobes based on rattle-structured upconverting luminescent nanoparticles, Angew. Chem., Int. Ed. 54 (27) (2015) 7915–7919.
[199] J. Yan, W.X. He, S.Q. Yan, F. Niu, T.Y. Liu, B.H. Ma, Y.P. Shao, Y.W. Yan, G. Yang, W.Y. Lu, Y.P. Du, B. Lei, P.X. Ma, Self-assembled peptide-lanthanide nanoclusters for safe tumor therapy: overcoming and utilizing biological barriers to peptide drug delivery, ACS Nano 12 (2) (2018) 2017–2026.
[200] X.L. Qi, Y.D. Han, S.J. Liu, H.F. Hu, Z.Z. Cheng, T.G. Liu, NaYF4:Yb/Tm@SiO2-Dox/Cur-CS/OSA nanoparticles with pH and photon responses, Nanotechnology 32 (25) (2021), 255703.
[201] M. Feng, Y.X. Wang, B. Lin, X.R. Peng, Y. Yuan, X.F. Tao, R.C. Lv, Degradable pH-responsive NIR-II imaging probes based on a polymer-lanthanide composite for chemotherapy, Dalton Trans. 49 (27) (2020) 9444–9453.
[202] N. Zhao, B.Y. Wu, X.L. Hu, D. Xing, NIR-triggered high-efficient photodynamic and chemo-cascade therapy using caspase-3 responsive functionalized upconversion nanoparticles, Biomaterials 141 (2017) 40–49.
[203] K. Ma, X.R. Wei, J. Liu, D.J. Chen, X.L. Zhao, J.W. Shen, H. Lu, P.X. Jia, Near-infrared-light-responsive nanocomposites of cell membrane mimetic copolymers and upconverting nanoparticles for on-demand drug release, ACS Appl. Nano Mater. 3 (8) (2020) 8294–8303.
[204] F.Y. Jin, J. Qi, M.X. Zhu, D. Liu, Y.C. You, G.F. Shu, Y. Du, J. Wang, H. Yu, M.C. Sun, X.L. Xu, Q.Y. Shen, X.Y. Ying, J.S. Ji, Y.Z. Du, NIR-triggered sequentially responsive nanocarriers amplified cascade synergistic effect of chemo-photodynamic therapy with inspired antitumor immunity, Acs Appl Mater Inter 12 (29) (2020) 32372–32387.
[205] F.J. Huang, R.L. Duan, Z.Z. Zhou, M. Vazquez-Gonzalez, F. Xia, I. Willner, Near-infrared light-activated membrane fusion for cancer cell therapeutic applications, Chem. Sci. 11 (21) (2020) 5592–5600.
[206] Y. Zhang, Z.Z. Yu, J.Q. Li, Y.X. Ao, J.W. Xue, Z.P. Zeng, X.L. Yang, T.T.Y. Tan, Ultrasmall-superbright neodymium-upconversion nanoparticles via energy migration manipulation and lattice modification: 808 nm-activated drug release, ACS Nano 11 (3) (2017) 2846–2857.
[207] L.Y. Ming, L. Song, J.X. Xu, R.P. Wang, J.P. Shi, M. Chen, Y. Zhang, Smart manganese dioxide-based lanthanide nanoprobes for triple-negative breast cancer precise gene synergistic chemodynamic therapy, Acs Appl Mater Inter 13 (30) (2021) 35444–35455.
[208] Z. Feng, T. Tang, T.X. Wu, X.M. Yu, Y.H. Zhang, M. Wang, J.Y. Zheng, Y.Y. Ying, S.Y. Chen, J. Zhou, X.X. Fan, S.L. Li, M.X. Zhang, J. Qian, Perfecting and extending the near-infrared imaging window, Light Sci. Appl. 10 (1) (2021) 197.